IRIS AperTO

UNIVERSITÀ DEGLI STUDI DI TORINO

AperTO - Archivio Istituzionale Open Access dell'Università di Torino

In vivo silencing of miR-125a-3p promotes myelin repair in models of white matter demyelination

This is the author's manuscript

Original Citation:

Availability:

This version is available http://hdl.handle.net/2318/1733599 since 2020-03-13T01:16:45Z

Published version:

DOI:10.1002/glia.23819

Terms of use:

Open Access

Anyone can freely access the full text of works made available as "Open Access". Works made available under a Creative Commons license can be used according to the terms and conditions of said license. Use of all other works requires consent of the right holder (author or publisher) if not exempted from copyright protection by the applicable law.

(Article begins on next page)

25 April 2024

Title

In vivo silencing of miR-125a-3p promotes myelin repair in models of white matter demyelination

Running title

MiR-125a-3p in demyelination

Authors

Davide Marangon[1], Enrica Boda[2,3], Roberta Parolisi[2,3], Camilla Negri[1], Corinna Giorgi[4], Francesca Montarolo[3,5], Simona Perga[3,5], Antonio Bertolotto[3,5], Annalisa Buffo[2,3], Maria P. Abbracchio[1,#], Davide Lecca[1,#,*].

[1]Department of Pharmacological and Biomolecular Science, Università degli Studi di Milano, Via Balzaretti 9, 20133 Milano, Italy.

[2]Department of Neuroscience Rita Levi Montalcini, University of Turin

[3]Neuroscience Institute Cavalieri Ottolenghi, Regione Gonzole 10, 10043 Orbassano, Italy.

[4]European Brain Research Institute, Viale Regina Elena 295, 00161 Rome, Italy

[5]Neurobiology Unit, Neurology-CReSM (Regional Referring Center of Multiple Sclerosis), AOU San Luigi Gonzaga, Regione Gonzole 10, 10043 Orbassano, Italy.

[*]Corresponding author

[#] Equally contributing

Acknowledgements

This work was supported by Fondazione Cariplo, grant no. 2014-1207 to DL and EB, Università degli Studi di Milano (Piano di Sostegno alla Ricerca 2015–17–LINEA 2 to DL), and by the "Department of Excellence" grant program from the Italian Ministry of Research (MIUR), granted to the Department of Pharmacological and Biomolecular Science, of the University of Milan, and to the Department of Neuroscience Rita Levi Montalcini of the University of Turin. The funders had no role in study design, data collection and analysis, decision to publish, or preparation of the manuscript. Tissue samples and associated clinical and neuropathological data were supplied by the Multiple Sclerosis Society Tissue Bank, funded by the Multiple Sclerosis Society of Great Britain and Northern Ireland, registered

charity 207495. The authors also thank Prof. Francesca Boscia (University of Naples) for fruitful discussion.

Conflict of Interest

The authors declare that they have no conflict of interest.

Data Availability Statement

The data that support the findings of this study are openly available in GEO profile at https://www.ncbi.nlm.nih.gov/geo/query/acc.cgi?acc=GSE143876

Word count

Acknowledgments: 124 words

Abstract: 193 words

Introduction: 487 words

Materials and methods: 2412 words

Results: 1708 words

Discussion: 1512 words

References: 1519 words

Figures: 5

Figure legends: 1074 words

Total word count: 9029 words

Abstract

In the last decade, microRNAs have been increasingly recognized as key modulators of glial development. Recently, we identified miR-125a-3p as a new player in oligodendrocyte physiology, regulating in vitro differentiation of oligodendrocyte precursor cells (OPCs). Here, we show that miR-125a-3p is up-regulated in active lesions of multiple sclerosis (MS) patients and in OPCs isolated

from the spinal cord of chronic experimental autoimmune encephalomyelitis (EAE) mice, but not in those isolated from the spontaneously remyelinating corpus callosum of lysolecithin-treated mice. To test whether a sustained expression of miR-125a-3p in OPCs contribute to defective remyelination, we modulated miR-125a-3p expression in vivo and ex-vivo after lysolecithin-induced demyelination. We found that lentiviral over-expression of miR-125a-3p impaired OPC maturation, whereas its downregulation accelerated remyelination. Transcriptome analysis and luciferase reporter assay revealed that these effects are partly mediated by the direct interaction of miR-125a-3p with Slc8a3, a sodium-calcium membrane transporter, and identified novel candidate targets, such as Gas7, that we demonstrated necessary to correctly address oligodendrocytes to terminal maturation. These findings show that miR-125a-3p upregulation negatively affects OPC maturation in vivo, suggest its role in the pathogenesis of demyelinating diseases and unveil new targets for future promyelinating protective interventions.

Keywords: miRNA/multiple sclerosis/oligodendrocyte/remyelination/WM lesion

Main Points

1. miR-125a-3p is upregulated in OPCs isolated from EAE mice spinal cord and in human active lesions.
2. miR-125a-3p inhibition promotes remyelination in an animal model of demyelination.
3. miR-125a-3p impairs OPC maturation by targeting Slc8a3 and Gas7.

Table of Contents Image (TOCI)

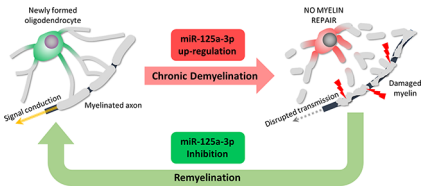

Introduction

Multiple sclerosis (MS) is a chronic immune-mediated demyelinating disease of the central nervous system (CNS) in which immune cells attack myelin, a fatty substance produced by oligodendrocytes that normally enwraps axons allowing proper transmission of nerve impulses. Currently, most of the available drugs are immunomodulators that, by targeting immune cells, can efficiently modify disease development reducing the number or the severity of attacks in relapsing-remitting MS.

However, these therapies are ineffective in the more severe progressive forms characterized by impaired remyelination, axonal degeneration and neuronal damage (Ghasemi, Razavi, & Nikzad, 2017). In this respect, fostering endogenous myelin repair represents a promising and yet unexploited therapeutic approach to MS.

To achieve successful remyelination, oligodendrocyte precursor cells (OPCs) respond to damage by enhancing their proliferation, migrating to the lesion site, differentiating and ensheathing denuded axons (Munzel & Williams, 2013). These processes occur with a relatively high efficiency after acute damage, but appear defective in chronic demyelinating diseases (Franklin & Ffrench-Constant, 2017). Analysis of post-mortem MS brain tissues show that most of the lesions are enriched in OPCs, suggesting that boost in precursor proliferation and migration is not followed by successful maturation and myelination (Kuhlmann, Lassmann, & Bruck, 2008; Lucchinetti et al., 1999). The identification of new molecular players regulating these processes could set the basis for the design of novel pharmacological interventions. OPC differentiation and maturation are influenced by both extrinsic (e.g. extracellular matrix, myelin components or pro-inflammatory cytokines; (Bonfanti et al., 2017; Coppolino et al., 2018; Harlow & Macklin, 2014; Mei, Christin Chong, & Chan, 2013) and intrinsic factors (e.g. transcriptional regulators and epigenetic factors; (Emery & Lu, 2015)).

In this regard, we recently identified miR-125a-3p as a negative regulator of oligodendrocyte differentiation (Lecca et al., 2016). Over-expression of miR-125a-3p in primary rat OPCs impaired, whereas its silencing enhanced cell maturation. We also showed miR-125a-3p levels to be up-regulated in the cerebrospinal fluid (CSF) of MS patients. Despite this initial evidence, the role of miR-125a-3p during *in vivo* demyelination and remyelination has never been investigated in detail. Further, miR-125a-3p targets mediating these effects are totally unknown.

Here, we show that miR-125a-3p is up-regulated in white matter (WM) active lesions of MS patients and in OPCs isolated from spinal cord of experimental autoimmune encephalomyelitis (EAE) mice at chronic phases, but not in OPCs isolated from the spontaneously repairing WM after lysolecithin (LPC)-induced demyelination. We also show that miR-125a-3p over-expression after demyelination impairs OPC maturation, whereas its silencing accelerates lesion repair. Our transcriptomic data suggest these effects are partly mediated by the direct interaction of miR-125a-3p with Slc8a3, a sodium-calcium membrane transporter up-regulated during oligodendrocyte maturation (Boscia et al., 2013). Furthermore, we identify the growth arrest-specific protein GAS7 as one of miR-125a-3p targets and describe, for the first time, its involvement in oligodendrocyte development. Together,

these findings support the view that the increased levels of miR-125a-3p observed in CSF and brain lesions of MS patients can contribute to defective remyelination.

Materials and Methods

Human post-mortem snap-frozen brain tissue blocks

Human post-mortem brain tissues were obtained from the United Kingdom (UK) MS Tissue Bank at Imperial College via a UK prospective donor scheme with full ethical approval (08/MRE09/31). Neuropathological confirmation of the diagnosis of MS was carried out according to the International Classification of Diseases of the Nervous System criteria (www.ICDNS.org), and confounding pathologies were excluded, including Alzheimer-like changes (Reynolds et al., 2011).

The project has been approved by the University Bioethics Committee of the University of Turin on 28 February 2015. Demographic, clinical, autopsy, and neuropathological characteristics of CC, SPMS and PPMS cases analyzed are summarized in Table S1.

Neuropathological characterization of human post-mortem snap-frozen brain tissue

The human post-mortem snap-frozen brain tissue blocks/slices from CC and MS patients were characterized for the presence of white matter (WM) and grey matter (GM), for the occurrence and extension of demyelinated lesions in WM (WML, including active lesions –AL, and chronic active lesions - CAL) and GM (GML) and for the degree of lesion activity using anti-MOG and anti-MHC antibodies respectively in immunohistochemical (IHC) reactions.

Total RNA extraction, retrotranscription and miRNA expression analysis from human brain tissues

For RNA extraction, 50-µm-thick cryosections cut from selected snap-frozen tissue blocks from CC and MS cases were used to manually dissect the area of normal appearing WM and GM with normal appearance and matched active lesions in WM and GM respectively based on immunohistochemistry characterization. The dissection was performed by gently incising the frozen tissue blocks (after characterization with anti-MOG and anti-MHCII antibodies) with a needle, before performing the cut of the tissue block. Two or three cryoslices were obtained from each tissue block, depending of the size of the area of interest.

Total RNA (including small RNAs) were extracted from the cryoslices using the Direct-zol RNA Kit (#R2060, Zymo Research, Irvine, CA), according to the manufacturer's instruction preceded by a

separation with phenol-chloroform. MiRNAs were reverse-transcribed at final concentration of 0,67 ng/µL using TaqMan™ MicroRNA Reverse Transcription Kit (#4366596, Thermo Fisher Scientific), according manufacturer's instruction. MiRNA analysis was performed by real-time PCR using TaqMan miRNA assay (Thermo Fisher Scientific) and normalized using the expression levels of the small nuclear RNA U6. Expression levels of miRNAs were calculated by the comparative cycle threshold (Ct) method ($2^{-\Delta Ct}$).

Animal care and experimental design

For all animal studies, international (European law Dir. 2010/63/UE) and national (Italian law DL n. 26, 4th March 2014) guidelines for the care and use of animals were followed. All the procedures were approved by the Italian Ministry of Health (735-2015PR to DL, 1112/2016-PR to AB). Mice were housed in groups of 4, under a 12-hr light/12-hr dark cycle at 21°C, with food and water ad libitum. In all *in vivo* experiments we used wild-type mice (Charles River, Calco, Italy)

The experiments were designed in compliance with the ARRIVE guidelines. Control groups were included in all experiments, randomizing the procedures and applying blinded analysis when possible. Sample size was calculated with G-Power, considering a significant level of 0.05 and to reach a power between 0.80 and 0.90.

EAE induction

EAE was induced in 9-week-old female wild-type C57Bl/6 mice (Charles River) by subcutaneous immunization in the flanks and in the tail base with 200µg of myelin oligodendrocyte glycoprotein (MOG35-55, Espikem) in incomplete Freund's adjuvant (IFA, Sigma-Aldrich) supplemented with 8 mg/ml of Mycobacterium tuberculosis (strain H37Ra, Difco). The immunized mice received intravenously 500 ng of pertussis toxin (PTX, Duotech) the day of the immunization and 48 hours later. Animals were daily weighted and scored for clinical symptoms of EAE according to the following scale (clinical score, CS): 0 = healthy, 1 = flaccid tail, 2 = ataxia and/or paresis of hindlimbs, 3 = paralysis of hindlimbs and/or paresis of forelimbs, 4= tetraparalysis, 5 =moribund or death. Non-EAE age-matched controls received PTX injections, as well as the initial injections of emulsion, but without the encephalitogen. The animals were sacrificed 50 days post immunization (dpi).

Design and generation of lentiviral vectors

Lentiviral plasmids pLB-miR-125a-GFP and pLB-ctrl-GFP were designed to obtain overexpression of miR125 or of a non-targeting control RNA respectively. The plasmids were cloned inserting the pre-miR125 (or pre-miR ctrl) dsDNA sequences into the HpaI e XhoI sites of the pLB lentiviral plasmid, under the control of the U6 promoter. The sense strand of the cloned fragments is as follows:

pre-miR125: TGACAGGTGAGGTTCTTGGGAGCCTTCAAGAGAGGCTCCCAAGAACCTCACCTGTTTTTTC

pre-miR ctrl: TGCAACAAGATGAAGAGCACCAACTCGAGTTGGTGCTCTTCATCTTGTTGCTTTTTC

To produce third generation lentiviral particles LV-miR-125a-GFP and LV-ctrl-GFP, Hek293T cells were $CaPO_4$ transfected with the corresponding lentiviral plasmid (either pLB-miR-125a-GFP or pLB-ctrl-GFP) and three packaging plasmids. At 48 and 72 hours from transfection, the growth media containing lentiviral particles was filtered (0.4 mm pore size) and subjected to ultracentrifugation at 26000 rpm for 1.5 hr in a SW40Ti rotor. Pelleted virions were resuspendend in PBS, aliquoted and stored at -80°C. Viral Titer (in transducing units: TU) was tested for each preparation, and varied between $1,7x10^8$ TU/ml and $1,0x10^9$ TU/ml. *In vitro* analyses on glial mixed cultures showed a ~ 25-fold increase in miR-125a-3p expression in cells transduced with LV-miR-125a-GFP compared to LV-ctrl-GFP (Fig. S2).

To inhibit miR-125a-3p function, lentiviral (LV) transduction particles were purchased from Sigma-Aldrich (MLTUD0027, MISSION® Lenti microRNA Inhibitor, Mouse, mmu-miR-125a-3p; HLTUD001C MISSION® Lenti microRNA Inhibitor, ath-miR416, Negative Control). Expression of the miRNA inhibitor is driven by the U6 promoter and exploits the tough decoy (TuD) technology (i.e. targeted miRNA suppression is achieved in a sequence specific manner by antisense RNA "decoy" molecules). Such LV particles are pseudotyped with an envelope G glycoprotein from Vesicular Stomatitis Virus (VSV-G). No reporter gene is comprised in such LV miRNA inhibitor vectors.

Acute LPC-mediated demyelination and in vivo injections of lentivirus

Surgery and perfusions were carried out under deep general anesthesia (ketamine, 100 mg/kg; Ketavet, Bayern, Leverkusen, Germany; xylazine, 5 mg/kg; Rompun; Bayer, Milan, Italy).

Acute demyelination was obtained in 3-4 month-old C57BL/6 mice by a bilateral stereotaxic microinjection of 1ul of a 1% lysolecithin (lysophosphatidylcholine, LPC, Sigma-Aldrich) in 0.9% NaCl solution into the subcortical white matter at coordinates: 1 mm medio-lateral, 0.1 mm rostral to bregma and at 1.2 from the cortical surface. One ul of LV particles ($1\times10^{9-10}$ TU/ml) was pressure-injected at the same coordinates at 5 (in case of LV-decoy-miR-125a-3p and relative LV-ctrl) or 9 days (in case of LV-overexpressing-miR-125a-3p and relative LV-ctrl) after lesion.

MACS sorting

OPCs have been isolated from the subcortical white matter of LPC/saline-injected mice at 5dpl and from the lumbar spinal cord of EAE mice at 50dpi. After tissue dissociation with a papain+DNAse solution (papain 1.5 mg/ml, L-cysteine 360 µg/ml, DNAse I 60 µg/ml in MEM; all from Sigma-Aldrich, Saint Louis, MS, USA), mouse OPCs were enriched by positive selection using an anti-PDGFRα antibody conjugated to magnetic beads, according to the instructions of the manufacturer (Miltenyi Biotech GmbH, Bergisch Gladbach, DE). MACSorted OPCs were collected in TRIzol Reagent (Invitrogen Life Technologies, NY, USA) and then processed for quantitative RT-PCR analysis (see below). Purity of the MACS-selected OPCs was verified by immunocytochemistry (more than 95% of the cells were $NG2^+$ at 6 hours post-plating).

Histology and immunofluorescence on fixed tissues

21 days after LPC-induced lesion (dpl), animals were anesthetized (as above) and transcardially perfused with 4% paraformaldehyde (PFA) in 0.1M phosphate buffer (PB). Brains were postfixed for 2 h, cryoprotected, and processed according to standard immunohistological procedures (Boda et al., 2015). Brain slices were stained to detect the expression of different antigens: GFP (1:700, Invitrogen); Sox10 (1:2000, Santa Cruz); NG2 (1:200, Millipore); GST-pi (1:500, Eppendorf). 4,6-diamidino-2-phenylindole (DAPI, Fluka, Milan, Italy) was used to counterstain cell nuclei. Myelin silver nitrate Gallyas staining was performed as in (Pistorio, Hendry, & Wang, 2006).

Image analysis

Quantitative evaluations (marker coexpression in GFP-tagged infected cells) were performed on confocal images by employing Neurolucida (MicroBrightfield, Colchester, VT) or ImageJ (Research Service Branch, National Institutes of Health, Bethesda, MD; available at: http://rsb.info.nih.gov/ij/). Measurements derived from at least 5 sections per animal. At least four animals were analyzed for each experimental condition. Adobe Photoshop 6.0 (Adobe Systems, San Jose, CA) was used to adjust image contrast and assemble the final plates.

Cerebellar organotypic slices

250 µm-thick parasagittal slices of postnatal day 10 (P10) mouse cerebellum were cut using a Tissue Chopper. The slices were placed on Millicell-CM culture plate inserts (Millipore) in a pro-survival

medium composed by 50% basal medium with Earle's salts, 25% Hanks' buffered salt solution, 25% horse serum, and 5 mg/ml glucose for at 37°C. One day after preparation, the slices were infected by adding one ul of LV-decoy-miR-125a-3p/ctrl particles (1×10^{10} TU/ml) in the medium. For the induction of demyelination, at 4 days *in vitro* (DIV) slices were incubated with fresh medium including 0.5 mg/ml LPC overnight (15–17 hr) at 37°C. After incubation, the LPC-containing medium was replaced with fresh medium. Slices from 3 millicells were pooled and lysed together 7-days post-demyelination with 500 µl of TRIzol Reagent (Invitrogen, NY, USA) for the subsequent RNA extraction.

OPC isolation and transfection

Mixed glial cultures were obtained from 12 postnatal day 2 (P2) Sprague-Dawley rat cerebral cortices pooled together as previously described (Lecca et al., 2016). OPCs were plated onto poly-D,L-ornithine-coated (final concentration 50 µg/ml; Sigma-Aldrich) 13-mm glass coverslips for immunocytochemistry (1-2 x 10^4 cells/coverslip) and poly-D,L-ornithine-coated 6-wells plates (10^5 cells/coverslip) or 6-cm dishes (2 x 10^5 cells/coverslip) for qRT-PCR assays. Cells were plated in Neurobasal medium supplemented with 2% B27 (Life Technologies), 2 mM L-glutamine, 10 ng/ml human platelet-derived growth factor BB (Sigma-Aldrich), and 10 ng/ml human basic fibroblast growth factor (Life Technologies) to promote proliferation. When OPCs reached a 60% confluency, cultures were switched to a Neurobasal medium lacking growth factors and containing triiodothyronine 15 nM (T3, Sigma-Aldrich) up to 4 days to allow differentiation. For transfection experiments, immediately after switching from proliferating to differentiating medium, OPCs were transfected with miR-125a-3p mimics (Dharmacon) or Gas7/Nod1 stealth siRNA (Life Technologies) at the final concentration of 50 nM with Lipofectamine RNAiMAX reagent (Life Technologies), following the manufacturer's protocol. A scrambled RNA transfection was included as negative control. Analysis were performed 48 hours after transfection.

Immunocytochemistry and cell counting

Cells were fixed in a 4% paraformaldehyde phosphate-buffered solution containing 4% sucrose. Incubation of anti-MBP primary antibody (1:200; Merck Millipore) was performed 2.5 hours at room temperature or over-night at 4°C. Cells were then incubated for 1 h at room temperature with secondary antibodies conjugated to AlexaFluor 555 (1:600; Life Technologies). The antibodies were diluted in a phosphate-buffered blocking solution (pH 7.4) containing 0.3% Triton X-100. Nuclei were labelled with the UV fluorescent dye Hoechst 33258 (1:10,000; Life Technologies). Coverslips were

then mounted in a fluorescent mounting medium (Dako). Positive cells for the selected markers were counted from 20 random fields for each coverslip (0.07 mm^2/field). The result was expressed as a percentage over the number of nuclei, and then normalized versus control (transfected with negative RNA), set to 100%.

Total RNA extraction, retrotranscription and gene expression analysis from rodent samples

Total RNA was extracted from rodent cells or tissues by using Direct-zol RNA micro- or mini-prep kit (Zymo Research). For qRT-PCR of miRNA, 10 ng of total RNA was reverse-transcribed with TaqMan® MicroRNA Reverse Transcription Kit and then subjected to Taqman microRNA assay (Life Technologies). Expression level of miR-125a-3p was normalized to the U87 snRNA in rat samples and to the U6 snRNA in mouse samples by the ΔCt method. For gene expression analysis, cDNA synthesis was performed starting from 400-800 ng of total RNA using SensiFAST™ cDNA synthesis kit (Bioline). The expression of all genes was analysed with SensiFAST™ SYBR Supermix (Bioline) and normalized to GAPDH expression using CFX96 real time PCR system (Bio-rad) following the manufacturer's protocol.

Transcriptome profiling and microarray analysis

RNA quality was assessed with Agilent 2100 Bioanalyzer (Agilent Technologies). RNA with RNA integrity number (RIN) > 7 was used for microarray analyses. Labelled cRNA was synthesized from 100 ng of total RNA using the Low Input Quick-Amp Labelling Kit, one colour (Agilent Technologies) in the presence of cyanine 3-CTP. Total RNA was hybridized on SurePrint G3 Rat Gene Expression Microarrays (#G4858A-074036, Agilent Technologies). This microarray consists of 60-mer DNA probes synthesized in situ, which represent 30,584 rat transcripts. Hybridization was performed at 65°C for 17 hours in a rotating oven (Microarray Facility, Laboratorio per le Tecnologie delle Terapie Avanzate, LTTA, Ferrara, Italy). One-color gene expression analysis was performed according to manufacturer's procedure. Feature Extraction 10.7.3 software (Agilent Technologies) was used to obtain microarray raw data. A fold change of ±1.5 and a FDR-adjusted p-value < 0.05 were considered to obtain the list of genes differentially expressed between the two experimental conditions. Datasets and raw data are publicly-available in GEO Profile (GEO ID: 200143876).

Site-directed mutagenesis

Slc8a3 and Gas7 3'UTR mutant plasmids were produced by creating a mutation in the miR-125a-3p binding site using the QuickChange® lightning site-directed mutagenesis kit (Agilent Technologies,

Italy) following manufacturer's instructions. For Slc8a3, the putative miR-125a-3p binding site TCACCTG was mutated into TGTGGTG by using the following primer pair: 3'-CTGGACTCGGGGTCCTTGAACACCACTGGATCCGGGACC-5' and 5'-GACCTGAGCCCCAGGAACTTGTG GTGACCTAGGCCCTGG-3'. For Gas7, the putative miR-125a-3p binding site TCACCTG was mutated into TCTGGAG by using the following primer pair: 3'-CCCCTGAGGAGACACGAGACCTCAAGGAAGG ACGTCGAAG-5' and 3'-GGGGACTCCTCTGTGCTCTGGAGTTCCTTCCTGCAGCTTC-5'.

Luciferase reporter assay

The web tool RNA22 was used to identify the hypothetical binding sites for miR-125a-3p on Gas7 and Slc8a3 3'UTRs. The reporter plasmids containing the Firefly (Fluc, upstream to the UTR region) and Renilla (Rluc) luciferase genes were purchased form Genecopoeia (Rockville, USA). The Gas7 3' UTR has been broken up into shorter fragments and cloned into two constructs (Gas7-1 and Gas7-2) with overlapping sequence. 50 ng of plasmid (empty vector, Gas7-1, Gas7-2, Nod1, Slc8a3, Gas7-2-MUT, Slc8a3-MUT) were transfected together with miR-125a-3p mimics or scramble miRNA at the concentration of 50 nM in COS7 cells (15.000 cells per well). Cells were lysed 48 hours after transfection. Dual luciferase reporter assay was performed to evaluate the luminescence signal produced in the different conditions by using Dual luciferase reporter kit (Promega) following manufacturer's protocol. In each condition, the ratio of Fluc/Rluc was calculated and the Fluc/Rluc value for the scramble RNA was set as 100%.

Statistical analysis

Data are presented as mean ±SEM and analyzed with the GraphPad Prism 7.04 software. For all comparisons between two groups with a normal distribution, two-tailed unpaired Student t-test was performed. Two-tailed paired Student t-test was used for analysis on human samples. For multiple comparison of groups with a normal distribution, one-way analysis of variance (ANOVA) accompanied by Tukey's post-hoc test was used. Two-way ANOVA with Tukey's multiple comparisons test was used to analyze luciferase reporter assay data. $P < 0.05$ was considered as statistically significant.

Results

MiR-125a-3p is upregulated in OPCs under non-remyelinating conditions

In a previous study, we found an up-regulation of miR-125a-3p in the CSF of MS patients (Lecca et al., 2016). Here, to assess whether this alteration is related to changes in its abundance in the nervous tissue, we measured miR-125a-3p expression in post-mortem tissues obtained from patients with progressive MS. Demographic and clinical details of these subjects are reported in Table S1. Analysis was performed on white and grey matter in control subjects and normal appearing white/gray matter (NAWM/NAGM) and white/gray matter active lesions (WML/GML) in MS patients. Results showed that miR-125a-3p expression levels were specifically up-regulated in MS patients only in WML, compared to NAWM (Fig. 1A; p=0.054), and reached statistical significance using paired analysis for each patient (Fig. 1B; p=0.03).

To assess if miR-125a-3p levels are specifically altered in oligodendroglial cells during/after *in vivo* demyelination, we analyzed its expression in two well-established mouse models, namely LPC-induced demyelination and chronic EAE, which reproduce different aspects of MS pathology. The LPC model is indeed characterized by a demyelination phase followed by spontaneous remyelination sustained by resident OPCs, which upregulate pre-myelinating markers approximately 7 days after focal injury (Boda et al., 2011). In contrast, in EAE, OPCs are blocked at an immature stage and fail to repair damage (Coppolino et al., 2018).

To induce focal demyelination, the toxicant LPC was bilaterally injected in the corpus callosum. As expected, MBP levels decreased significantly at 5 days post-lesion (Fig. S1A). At the same time point, PDGFRα$^+$ OPCs were isolated by means of MACS sorting (Fig. 1C). A significant decrease in miR-125a-3p levels was found in OPCs isolated from LPC-treated animals compared to saline-treated group (Fig. 1D). In the EAE model, mice were immunized with a fragment of the MOG peptide (MOG 35-55). Analysis of clinical scores confirmed the expected disease development (Fig. S1B). Fifty days post-immunization, when the disease was in its chronic phase, mice were sacrificed and PDGFRα$^+$ OPCs were isolated from the lumbar region of the spinal cord (Fig. 1E). At variance with the LPC model, we observed a significant increase of miR-125a-3p in OPCs isolated from EAE mice compared to controls (Fig. 1F)

Overall, these data suggest that miR-125a-3p up-regulation may contribute to the pathogenetic mechanisms responsible for blockade of OPCs at immature stages and prevention of remyelination processes.

In vivo modulation of miR-125a-3p regulates the timing of oligodendroglia maturation after myelin damage

Based on these results, we next wondered whether high levels of miR-125a-3p could affect the outcome of demyelination in terms of oligodendrocyte maturation and/or myelin repair in a condition in which these processes spontaneously occur. To assess this hypothesis, we took advantage of the LPC-induced demyelination model described above (Fig. 2A).

LPC-treated animals were injected with lentiviral (LV) particles designed to overexpress our target miRNA (Fig. 2A). As expected, early after lesion (5 dpl) we observed an almost complete loss of myelin in the corpus callosum and in the white matter tracts under the cingulate and primary motor cortex (Fig. 2B). Consistently, the lesion area was completely deprived of mature GSTpi-positive (+) oligodendrocytes (Fig. 2C) and a high number of cells, including immature NG2$^+$ OPCs reacting to the injury were recruited to this site, as shown by the dense mass of DAPI$^+$ nuclei (Fig. 2D). To test the effects of miR-125a-3p overexpression, we generated LV particles co-expressing the miRNA and a GFP reporter under constitutive promoters (LV-miRNA-125a-GFP), or a non-targeting miRNA as control (LV-ctrl-GFP). The efficacy of the LV-mir-125a-GFP was tested by assessing the expression levels of miR-125a-3p after infection of mixed glial cells (Fig. S2). LV particles were injected in the parenchyma at 9 dpl, a stage in which demyelination is already evident and the recruited precursor cells start to differentiate. Mice were then sacrificed at 21 dpl, when OPC maturation is normally largely restored (Woodruff & Franklin, 1999). A significant number of infected (i.e. GFP$^+$) cells was found in white matter tracts in both conditions (Fig. 2E), mainly oligodendroglia (i.e. SOX10$^+$ cells, 20% of the infected cells; Fig. S3A) and astrocytes (80%, data not shown). LV-targeted oligodendroglia accounted for 10% of the total oligodendroglial population (SOX10$^+$, Fig. S3B). The number of infected oligodendrocytes was comparable within the two experimental groups (Fig. S3C, D), excluding a major effect of miR-125a-3p overexpression on post-injury oligodendroglia amplification. Upon infection with the control LV particles (LV-ctrl), about 70% of infected Sox10$^+$ cells were NG2-negative (Fig. 2F, H), and a significant fraction of them (about 40%) acquired a more branched phenotype and were positive for the mature marker GSTpi (Fig. 2G, I). In contrast, we observed that the vast majority (85%) of LV-miR-125a-GFP infected Sox10$^+$ oligodendroglial cells still displayed immature features (i.e. NG2 positivity and an OPC-like morphology; Fig. 2H) and that very few cells reached the GSTpi$^+$ stage (Fig. 2I). Such maturation defect was not observed in the GFP$^-$ oligodendroglial population (Fig. S3D), reinforcing the hypothesis of a cell-intrinsic effect mediated by miR-125a-3p over-expression in OPCs. Quantification of myelin staining in the corpus callosum did not show any statistical difference between miR-125a-infected mice and the control

group, likely due to the low proportion of infected oligodendrocytes over the total number of oligodendroglial cells.

Based on these results, we wondered whether miR-125a-3p silencing could instead accelerate the remyelination process after LPC-induced demyelination (Fig. 3A). Interestingly, the injection of LV particles designed to inhibit miR-125a-3p (LV-decoy-mir-125a) at 5 dpl resulted in a 2-fold increase of GSTpi$^+$ cell density (Fig. 3B-D), a slight increase in the total Sox10$^+$ oligodendroglial population (Fig. 3E) and in myelin production (Fig. 3 F-H) at 21 dpl, compared to control conditions (LV-ctrl). In line with these results, LV-mediated inhibition of miR-125a-3p in an *ex vivo* model of demyelination (i.e. LPC treatment in cerebellar organotypic cultures, Fig. 3I) was associated with a significant increase of the expression levels of early (i.e. NG2) and pre-myelinating (i.e. Olig1 and Gpr17) oligodendroglial markers and late myelin genes (i.e. Plp1 and Mbp) (Fig. 3J).

Altogether, these data suggest that miR-125a-3p silencing promotes post-injury oligodendroglia amplification and, to a larger extent, OPC maturation, consistent with our previous *in vitro* study (Lecca et al., 2016). They also suggest that *in vivo* manipulation of miR-125a-3p levels could be exploited to accelerate myelin repair after demyelination.

MiR-125a-3p inhibits OPC maturation by affecting Slc8a3 and Gas7 expression

To explore the mechanisms underlying the effects of miR-125a-3p on oligodendrocyte maturation, we performed a transcriptomic analysis of differentiating OPC cultures upon miR-125a-3p over-expression. We identified 1,060 significantly modulated genes, among which 480 were significantly down-regulated. By comparing this dataset with the already published list of the top-50 up-regulated genes during OPC differentiation (Dugas, Tai, Speed, Ngai, & Barres, 2006), we observed that most of them were indeed down-regulated, confirming a strong negative effect of miR-125a-3p on OPC maturation (Fig. 4A). Next, to identify new direct targets of miR-125a-3p, we identified which of these 480 genes were also putative miR-125a-3p targets (as predicted by MiRwalk, (Dweep & Gretz, 2015)) and up-regulated during physiological OPC maturation (Cahoy et al., 2008) (Fig. 4B). The 10 resulting candidate genes (Table S2) were further filtered based on the fold change and normalized abundance in OPCs, leading to the selection of two candidates, namely growth arrest specific 7 (Gas7) and nucleotide-binding oligomerization domain 1 (Nod1). Solute carrier family 8 member 3 (Slc8a3), encoding for the membrane transporter NCX3, was also selected from the list based on its recognized role in OPC maturation (Boscia et al., 2012). As a first step, we confirmed the down-regulation of Gas7, Nod1 and Slc8a3 transcripts by qPCR, in cultured OPCs after miR-125a-3p over-expression

(Fig. 4C). Then, we analyzed the expression levels of Gas7 and Nod1 during *in vitro* OPC maturation and found that they were progressively up-regulated up to 7-fold and 3-fold, respectively, compared to non-differentiated OPCs (Fig. 4D, E), suggesting that miR-125a-3p over-expression impairs OPC maturation by preventing the up-regulation of these targets.

To strengthen this hypothesis and assess the role of Gas7 and Nod1 as putative players in oligodendroglia differentiation, we reduced their expression during in vitro OPC maturation by transfecting specific small interfering RNAs (siRNAs). Silencing efficiency was assessed by qRT-PCR 48 hours after siRNA transfection (Fig. S4). Interestingly, we observed that Gas7 silencing led to a significant reduction in MBP transcript levels and in the number of MBP^+ oligodendrocytes, whereas Nod1 silencing only led to a trend in MBP^+ cells reduction (Fig. 5 A-F). Slc8a3 silencing has been already shown to impair oligodendrocyte terminal maturation (Boscia et al., 2013). Altogether, these results suggest that the pathogenetic mechanism induced by miR-125a-3p up-regulation may be due, at least in part, by an inhibitory effect on both Gas7 and Slc8a3.

To univocally assess the direct interaction of miR-125a-3p with Gas7, Nod1 and Slc8a3 transcripts, we performed a dual luciferase reporter assay. COS7 cells were co-transfected with a reporter plasmid containing the 3'UTR of Gas7 (cloned in two separate plasmids, namely Gas7-1 and Gas7-2, which contain an overlapping sequence), Nod1 or Slc8a3, downstream to the Firefly luciferase gene, together with the miR-125a-3p mimic or a scramble miRNA. The co-transfection of Gas7-2 and Slc8a3 construct with miR-125a-3p mimic led to a significant reduction in luciferase activity compared to the levels obtained with the scramble miRNA (Fig. 5G), whereas the reduction observed in case of Gas7-1 and Nod1 did not reach significance. These results indicate that miR-125a-3p can directly bind to the 3' UTR of Gas7 and Slc8a3, but not to that of Nod1.

Using the prediction tool Targetscan, we identified putative microRNA response elements (MREs) for miR-125a-3p in the 3'UTR of both Slc8a3 and Gas7 (Fig. 5H and Fig S5A). To assess whether miR-125a-3p can bind to these sequences we assessed the effect of site-directed mutagenesis on luciferase activity. The reporter assay demonstrated that mutation of the putative MRE in the Gas7 3'UTR (Fig. S5B) affected the luciferase activity in a miR-125a-3p-independent manner (Fig. S5C), suggesting the possible involvement of other regulatory mechanisms matching that sequence. On the contrary, mutation of the MRE in the Slc8a3 3'UTR (Fig. 5I) increased the luciferase activity and completely abolished the inhibitory effect of miR-125a-3p (Fig. 3J). Overall, these results indicate that miR-125a-3p can target both Gas7 and Slc8a3, even if, in the case of the Gas7 transcript, the MRE still needs to be identified.

Discussion

In recent years, miR-125a has emerged as an important regulator of different aspects of CNS development (Boissart, Nissan, Giraud-Triboult, Peschanski, & Benchoua, 2012; Lecca et al., 2016; Shenoy, Danial, & Blelloch, 2015). Our previous studies demonstrated that the -3p strand of this miRNA (miR-125a-3p) is involved in the regulation of OPC differentiation *in vitro*, showing that its over-expression impairs cell maturation (Lecca et al., 2016). Despite this first finding, the actual role of this miRNA in OPC maturation and myelination *in vivo*, the mechanism subserving its action, and the pathological relevance of its alterations in demyelinating conditions were totally unknown. Here, we addressed this gap by investigating miR-125a-3p expression levels in OPCs in two *in vivo* models of myelin injury with quite different outcomes (spontaneous remyelination in the lysolecithin-induced model and largely defective repair in the EAE model), and by evaluating the consequences of miR-125a-3p positive or negative modulation on myelin repair. Significant up-regulation of miR-125a-3p was observed in active lesions of MS patients and in OPCs isolated form EAE mice spinal cord, which are blocked at an immature stage (Coppolino et al., 2018; Girolamo et al., 2011), but not in OPCs isolated from the corpus callosum of lysolecithin-treated mice, in which spontaneous remyelination takes place (Woodruff & Franklin, 1999). These findings suggest that miR-125a-3p up-regulation could contribute to impair OPC terminal maturation and eventually to defective remyelination under chronic demyelinating conditions as those reproduced in EAE mice.

To tackle this issue, we over-expressed miR-125a-3p in mouse corpus callosum following lysolecithin-induced demyelination. LV particles were injected 9 dpl, a time window corresponding to the initiation of OPC differentiation, in order to investigate whether miR125a-3p overexpression would repress oligodendroglia maturation program (once it was already set up). To increase the probability to detect fine differences in lesion repair, the effects of this manipulation were investigated at 21 dpl, when OPC maturation is normally largely restored, but remyelination has not reached a plateau (Woodruff & Franklin, 1999). Interestingly, we found that miR-125a-3p over-expression maintained oligodendrocytes in the $NG2^+$ precursor stage and decreased the number of oligodendrocytes reaching the $GSTpi^+$ mature stage, consistent with a delay in OPC maturation and subsequent re-myelination. Such impairment in the maturation process was not detected in the non-infected oligodendroglial population, suggesting a cell-autonomous inhibitory effect of miR125a-3p in OPCs, and excluding a major role of cell-extrinsic factors due to miR125a-3p overexpression in other cell types (e.g., astrocytes, that were also largely targeted by LV). To assess the effects of miR-125a-3p silencing, we injected a LV-mediated miRNA inhibitor (decoy) at 5 dpl in the same

experimental model, in order to target recruited OPCs and possibly accelerate/de-repress their engagement in the differentiation program. Such manipulation resulted in a significant increase in the number of mature GSTpi oligodendrocytes, coupled with an increase in Gallyas myelin staining. The positive effects of miRNA silencing on myelination were also confirmed ex vivo, in LPC-treated organotypic cultures. While the effect of miR125a-3p overexpression can be reasonably attributed to cell-intrinsic mechanisms (see above), the lack of a reporter in LV-decoy constructs did not allow us to assess whether the effect of miR125a-3p silencing is direct or indirect (i.e., mediated by other cell types targeted by the LV construct). Nevertheless, these data suggest that the pharmacological inhibition of miR-125a-3p in the lesioned WM could represent a potential approach to foster endogenous remyelination.

As previously hypothesized, the inhibitory effect of miR-125a-3p is likely mediated by the interaction of this miRNA with several transcripts whose involvement in oligodendrocyte maturation has been already demonstrated or postulated (Boissart et al., 2012; Dong, Li, Ni, Zhao, & Liu, 2014; Lecca et al., 2016; Yin et al., 2015). By transcriptomic analysis, we identified new potential miR-125a-3p direct targets, and selected Gas7, Nod1 and Slc8a3 as the best candidates, based on their relative abundance in OPCs, strong fold decrease after miR-125a-3p over-expression and previous literature data. Slc8a3 encodes for a transmembrane Na^{+}/Ca^{2+} exchanger, called NCX3, recently identified as a myelin membrane component, involved in the regulation of $[Ca^{2+}]i$ in OPCs during differentiation and myelin synthesis (Boscia et al., 2016; Friess et al., 2016). NCX3 expression was shown to be up-regulated during oligodendrocyte maturation and its knock-down prevented the expression of the myelin proteins CNPase and MBP (Boscia et al., 2013). The growth-arrest protein Gas7 is a cytosolic protein mainly expressed in the brain, involved in the morphological differentiation and microfilament organization of several cell types (Chao, Hung, & Chao, 2013; Ju et al., 1998; She, Liou, & Lin-Chao, 2002). NOD1 belongs to the intracellular NOD-like receptor family, is widely expressed in several cell types (Rosenzweig, Galster, Planck, & Rosenbaum, 2009; Velloso, Sogayar, & Correa, 2018; L. Zhao, Hu, Zhou, Purohit, & Hwang, 2011) and has been implicated in dendritic cell activation and CNS infiltration, essential events associated with MS progression (Shaw et al., 2011). However, neither the expression nor the functions of Gas7 and Nod1 in oligodendrocytes had never been described before. Our data suggest their involvement in oligodendrocyte terminal maturation. Accordingly, silencing experiments confirmed that at least Gas7 is required for correct OPC maturation. Moreover, the validation of the direct interaction of miR-125a-3p with Gas7 and Slc8a3 3′-UTRs highlights a new mechanism of action through which miR-125a-3p contributes to impair

OPC differentiation and myelination. Nevertheless, since our expression profile has been performed on cultures of differentiating oligodendrocytes and not on brain tissue undergoing demyelination, it is formally possible that Gas7 and Slc8a3 are relevant target of miR-125a-3p only in developmental myelination and not in remyelination.

It is becoming increasingly clear that miRNA-mediated post-transcriptional mechanisms play an essential role in MS pathology. MiR-155 was found to be up-regulated in plasma (Zhang et al., 2014) and active lesions (Junker et al., 2009; Moore et al., 2013) of MS patients. Accordingly, administration of anti-miR-155 in the experimental autoimmune encephalomyelitis (EAE), a well-established mouse model of MS, significantly ameliorated clinical outcomes decreasing Th1 and Th17 responses in the CNS and peripheral lymphoid organs (Murugaiyan, Beynon, Mittal, Joller, & Weiner, 2011). Similarly, miR-326 was found to be up-regulated in MS active lesions and its expression highly correlated with MS patient's disability. Interestingly, miR-326 *in vivo* silencing reduced, whereas its over-expression increased, the number of Th17 cells and EAE severity (Du et al., 2009). In our previous study, we found a significant up-regulation of miR-125a-3p levels in the cerebrospinal fluid of MS patients in the relapsing phase (Lecca et al., 2016), suggesting that this was due to its release from neural cells, such as neurons or oligodendrocytes. Here, analysis of miRNA levels in human MS lesions compared to normal-appearing WM specimens strengthened this hypothesis and suggested that the pathological up-regulation of miR-125a-3p could be relevant to the development of the human disease, even though the exact mechanism is still unknown. Based on the observed up-regulation of miR-125a-3p in OPCs isolated from the spinal cord of EAE mice, we speculate that when miR-125a-3p levels are high, oligodendrocyte maturation is blocked leading to detrimental effects in demyelinating conditions. Interestingly, re-myelination failure in MS is frequently due to an impairment in the maturation of oligodendrocytes (Kuhlmann et al., 2008; Lucchinetti et al., 1999). In this respect, investigating miRNAs that regulate OPC differentiation and myelination should help identifying novel targets to foster endogenous re-myelination in MS patients. Several other miRNAs involved in OPC maturation and myelination have been found altered in MS samples, including miR-338 and miR-219, which were described strongly down-regulated in brain lesions and CSF from MS patients (Bruinsma et al., 2017; Junker et al., 2009). These miRNAs antagonize the expression of myelination inhibitors, and they are highly expressed in mature oligodendrocytes (Dugas et al., 2010; X. Zhao et al., 2010). The ability of miRNAs to simultaneously regulate the expression of multiple genes is the main feature that attracted the attention of researchers and clinicians to consider miRNAs as a new promising category of "drugs" (Marangon, Raffaele, Fumagalli, & Lecca, 2019).

However, given the high heterogeneity of cell types involved in MS pathogenesis and the intrinsic pleiotropic effect of miRNAs, understanding how a candidate miRNA may affect the phenotype of individual cell types in the CNS is a critical issue for the identification of new miRNA-based drugs for the treatment of MS. Previous studies have shown that also neuronal cells express miR-125a-3p (Lecca et al., 2016; Liu, Yin, Yan, Wang, & Luo, 2017) and reported its role in the regulation of the neurite outgrowth pathway (Liu et al., 2017). Thus, neurons represent another potential source of miR-125a-3p that may indirectly affect OPC development, for example, by releasing miRNA-containing exosomes and other types of extracellular vesicles (Raposo & Stoorvogel, 2013). Indeed, mutual interactions between neurons and oligodendrocytes are not only crucial for myelination, but also for long-term survival of axons (Fruhbeis et al., 2013; Piaton, Gould, & Lubetzki, 2010).

The identification of miR-125a-3p as a modulator of oligodendrocyte differentiation and myelination *in vivo* contributes to increase our understanding of the complex molecular machinery underlying de/re-myelination processes. Moreover, results from this study suggest that an antago-miRNA specific for miR-125a-3p could help promoting remyelination in diseases characterized by impaired myelin repair or disruption during development.

References

Boda, E., Di Maria, S., Rosa, P., Taylor, V., Abbracchio, M. P., & Buffo, A. (2015). Early phenotypic asymmetry of sister oligodendrocyte progenitor cells after mitosis and its modulation by aging and extrinsic factors. *Glia, 63*(2), 271-286. doi:10.1002/glia.22750

Boda, E., Vigano, F., Rosa, P., Fumagalli, M., Labat-Gest, V., Tempia, F., . . . Buffo, A. (2011). The GPR17 receptor in NG2 expressing cells: focus on in vivo cell maturation and participation in acute trauma and chronic damage. *Glia, 59*(12), 1958-1973. doi:10.1002/glia.21237

Boissart, C., Nissan, X., Giraud-Triboult, K., Peschanski, M., & Benchoua, A. (2012). miR-125 potentiates early neural specification of human embryonic stem cells. *Development, 139*(7), 1247-1257. doi:10.1242/dev.073627

Bonfanti, E., Gelosa, P., Fumagalli, M., Dimou, L., Vigano, F., Tremoli, E., . . . Abbracchio, M. P. (2017). The role of oligodendrocyte precursor cells expressing the GPR17 receptor in brain remodeling after stroke. *Cell Death Dis, 8*(6), e2871. doi:10.1038/cddis.2017.256

Boscia, F., Begum, G., Pignataro, G., Sirabella, R., Cuomo, O., Casamassa, A., . . . Annunziato, L. (2016). Glial Na(+) -dependent ion transporters in pathophysiological conditions. *Glia, 64*(10), 1677-1697. doi:10.1002/glia.23030

Boscia, F., D'Avanzo, C., Pannaccione, A., Secondo, A., Casamassa, A., Formisano, L., . . . Annunziato, L. (2013). New roles of NCX in glial cells: activation of microglia in ischemia and differentiation of oligodendrocytes. *Adv Exp Med Biol, 961*, 307-316. doi:10.1007/978-1-4614-4756-6_26

Boscia, F., D'Avanzo, C., Pannaccione, A., Secondo, A., Casamassa, A., Formisano, L., . . . Annunziato, L. (2012). Silencing or knocking out the Na(+)/Ca(2+) exchanger-3 (NCX3) impairs oligodendrocyte differentiation. *Cell Death Differ, 19*(4), 562-572. doi:10.1038/cdd.2011.125

Bruinsma, I. B., van Dijk, M., Bridel, C., van de Lisdonk, T., Haverkort, S. Q., Runia, T. F., . . . de Jong, B. A. (2017). Regulator of oligodendrocyte maturation, miR-219, a potential biomarker for MS. *J Neuroinflammation, 14*(1), 235. doi:10.1186/s12974-017-1006-3

Cahoy, J. D., Emery, B., Kaushal, A., Foo, L. C., Zamanian, J. L., Christopherson, K. S., . . . Barres, B. A. (2008). A transcriptome database for astrocytes, neurons, and oligodendrocytes: a new resource for understanding brain development and function. *J Neurosci, 28*(1), 264-278. doi:10.1523/JNEUROSCI.4178-07.2008

Chao, C. C., Hung, F. C., & Chao, J. J. (2013). Gas7 is required for mesenchymal stem cell-derived bone development. *Stem Cells Int, 2013*, 137010. doi:10.1155/2013/137010

Coppolino, G. T., Marangon, D., Negri, C., Menichetti, G., Fumagalli, M., Gelosa, P., . . . Abbracchio, M. P. (2018). Differential local tissue permissiveness influences the final fate of GPR17-expressing oligodendrocyte precursors in two distinct models of demyelination. *Glia, 66*(5), 1118-1130. doi:10.1002/glia.23305

Dong, Y., Li, P., Ni, Y., Zhao, J., & Liu, Z. (2014). Decreased microRNA-125a-3p contributes to upregulation of p38 MAPK in rat trigeminal ganglions with orofacial inflammatory pain. *PLoS One, 9*(11), e111594. doi:10.1371/journal.pone.0111594

Du, C., Liu, C., Kang, J., Zhao, G., Ye, Z., Huang, S., . . . Pei, G. (2009). MicroRNA miR-326 regulates TH-17 differentiation and is associated with the pathogenesis of multiple sclerosis. *Nat Immunol, 10*(12), 1252-1259. doi:10.1038/ni.1798

Dugas, J. C., Cuellar, T. L., Scholze, A., Ason, B., Ibrahim, A., Emery, B., . . . Barres, B. A. (2010). Dicer1 and miR-219 Are required for normal oligodendrocyte differentiation and myelination. *Neuron, 65*(5), 597-611. doi:10.1016/j.neuron.2010.01.027

Dugas, J. C., Tai, Y. C., Speed, T. P., Ngai, J., & Barres, B. A. (2006). Functional genomic analysis of oligodendrocyte differentiation. *J Neurosci, 26*(43), 10967-10983. doi:10.1523/JNEUROSCI.2572-06.2006

Dweep, H., & Gretz, N. (2015). miRWalk2.0: a comprehensive atlas of microRNA-target interactions. *Nat Methods, 12*(8), 697. doi:10.1038/nmeth.3485

Emery, B., & Lu, Q. R. (2015). Transcriptional and Epigenetic Regulation of Oligodendrocyte Development and Myelination in the Central Nervous System. *Cold Spring Harb Perspect Biol, 7*(9), a020461. doi:10.1101/cshperspect.a020461

Franklin, R. J. M., & Ffrench-Constant, C. (2017). Regenerating CNS myelin - from mechanisms to experimental medicines. *Nat Rev Neurosci, 18*(12), 753-769. doi:10.1038/nrn.2017.136

Friess, M., Hammann, J., Unichenko, P., Luhmann, H. J., White, R., & Kirischuk, S. (2016). Intracellular ion signaling influences myelin basic protein synthesis in oligodendrocyte precursor cells. *Cell Calcium, 60*(5), 322-330. doi:10.1016/j.ceca.2016.06.009

Fruhbeis, C., Frohlich, D., Kuo, W. P., Amphornrat, J., Thilemann, S., Saab, A. S., . . . Kramer-Albers, E. M. (2013). Neurotransmitter-triggered transfer of exosomes mediates oligodendrocyte-neuron communication. *PLoS Biol, 11*(7), e1001604. doi:10.1371/journal.pbio.1001604

Ghasemi, N., Razavi, S., & Nikzad, E. (2017). Multiple Sclerosis: Pathogenesis, Symptoms, Diagnoses and Cell-Based Therapy. *Cell J, 19*(1), 1-10. doi:10.22074/cellj.2016.4867

Girolamo, F., Ferrara, G., Strippoli, M., Rizzi, M., Errede, M., Trojano, M., . . . Virgintino, D. (2011). Cerebral cortex demyelination and oligodendrocyte precursor response to experimental autoimmune encephalomyelitis. *Neurobiol Dis, 43*(3), 678-689. doi:10.1016/j.nbd.2011.05.021

Harlow, D. E., & Macklin, W. B. (2014). Inhibitors of myelination: ECM changes, CSPGs and PTPs. *Exp Neurol, 251*, 39-46. doi:10.1016/j.expneurol.2013.10.017

Ju, Y. T., Chang, A. C., She, B. R., Tsaur, M. L., Hwang, H. M., Chao, C. C., . . . Lin-Chao, S. (1998). gas7: A gene expressed preferentially in growth-arrested fibroblasts and terminally differentiated Purkinje neurons affects neurite formation. *Proc Natl Acad Sci U S A, 95*(19), 11423-11428. doi:10.1073/pnas.95.19.11423

Junker, A., Krumbholz, M., Eisele, S., Mohan, H., Augstein, F., Bittner, R., . . . Meinl, E. (2009). MicroRNA profiling of multiple sclerosis lesions identifies modulators of the regulatory protein CD47. *Brain, 132*(Pt 12), 3342-3352. doi:10.1093/brain/awp300

Kuhlmann, T., Lassmann, H., & Bruck, W. (2008). Diagnosis of inflammatory demyelination in biopsy specimens: a practical approach. *Acta Neuropathol, 115*(3), 275-287. doi:10.1007/s00401-007-0320-8

Lecca, D., Marangon, D., Coppolino, G. T., Mendez, A. M., Finardi, A., Costa, G. D., . . . Abbracchio, M. P. (2016). MiR-125a-3p timely inhibits oligodendroglial maturation and is pathologically up-regulated in human multiple sclerosis. *Sci Rep, 6*, 34503. doi:10.1038/srep34503

Liu, J. Z., Yin, F. Y., Yan, C. Y., Wang, H., & Luo, X. H. (2017). Regulation of Docetaxel Sensitivity in Prostate Cancer Cells by hsa-miR-125a-3p via Modulation of Metastasis-Associated Protein 1 Signaling. *Urology, 105*, 208 e211-208 e217. doi:10.1016/j.urology.2017.01.001

Lucchinetti, C., Bruck, W., Parisi, J., Scheithauer, B., Rodriguez, M., & Lassmann, H. (1999). A quantitative analysis of oligodendrocytes in multiple sclerosis lesions. A study of 113 cases. *Brain, 122 (Pt 12)*, 2279-2295. doi:10.1093/brain/122.12.2279

Marangon, D., Raffaele, S., Fumagalli, M., & Lecca, D. (2019). MicroRNAs change the games in central nervous system pharmacology. *Biochem Pharmacol, 168*, 162-172. doi:10.1016/j.bcp.2019.06.019

Mei, F., Christin Chong, S. Y., & Chan, J. R. (2013). Myelin-based inhibitors of oligodendrocyte myelination: clues from axonal growth and regeneration. *Neurosci Bull, 29*(2), 177-188. doi:10.1007/s12264-013-1319-x

Moore, C. S., Rao, V. T., Durafourt, B. A., Bedell, B. J., Ludwin, S. K., Bar-Or, A., & Antel, J. P. (2013). miR-155 as a multiple sclerosis-relevant regulator of myeloid cell polarization. *Ann Neurol, 74*(5), 709-720. doi:10.1002/ana.23967

Munzel, E. J., & Williams, A. (2013). Promoting remyelination in multiple sclerosis-recent advances. *Drugs, 73*(18), 2017-2029. doi:10.1007/s40265-013-0146-8

Murugaiyan, G., Beynon, V., Mittal, A., Joller, N., & Weiner, H. L. (2011). Silencing microRNA-155 ameliorates experimental autoimmune encephalomyelitis. *J Immunol, 187*(5), 2213-2221. doi:10.4049/jimmunol.1003952

Piaton, G., Gould, R. M., & Lubetzki, C. (2010). Axon-oligodendrocyte interactions during developmental myelination, demyelination and repair. *J Neurochem, 114*(5), 1243-1260. doi:10.1111/j.1471-4159.2010.06831.x

Pistorio, A. L., Hendry, S. H., & Wang, X. (2006). A modified technique for high-resolution staining of myelin. *J Neurosci Methods, 153*(1), 135-146. doi:10.1016/j.jneumeth.2005.10.014

Raposo, G., & Stoorvogel, W. (2013). Extracellular vesicles: exosomes, microvesicles, and friends. *J Cell Biol, 200*(4), 373-383. doi:10.1083/jcb.201211138

Reynolds, R., Roncaroli, F., Nicholas, R., Radotra, B., Gveric, D., & Howell, O. (2011). The neuropathological basis of clinical progression in multiple sclerosis. *Acta Neuropathol, 122*(2), 155-170. doi:10.1007/s00401-011-0840-0

Rosenzweig, H. L., Galster, K. T., Planck, S. R., & Rosenbaum, J. T. (2009). NOD1 expression in the eye and functional contribution to IL-1beta-dependent ocular inflammation in mice. *Invest Ophthalmol Vis Sci, 50*(4), 1746-1753. doi:10.1167/iovs.08-2852

Shaw, P. J., Barr, M. J., Lukens, J. R., McGargill, M. A., Chi, H., Mak, T. W., & Kanneganti, T. D. (2011). Signaling via the RIP2 adaptor protein in central nervous system-infiltrating dendritic cells promotes inflammation and autoimmunity. *Immunity, 34*(1), 75-84. doi:10.1016/j.immuni.2010.12.015

She, B. R., Liou, G. G., & Lin-Chao, S. (2002). Association of the growth-arrest-specific protein Gas7 with F-actin induces reorganization of microfilaments and promotes membrane outgrowth. *Exp Cell Res, 273*(1), 34-44. doi:10.1006/excr.2001.5435

Shenoy, A., Danial, M., & Blelloch, R. H. (2015). Let-7 and miR-125 cooperate to prime progenitors for astrogliogenesis. *EMBO J, 34*(9), 1180-1194. doi:10.15252/embj.201489504

Velloso, F. J., Sogayar, M. C., & Correa, R. G. (2018). Expression and in vitro assessment of tumorigenicity for NOD1 and NOD2 receptors in breast cancer cell lines. *BMC Res Notes, 11*(1), 222. doi:10.1186/s13104-018-3335-4

Woodruff, R. H., & Franklin, R. J. (1999). The expression of myelin protein mRNAs during remyelination of lysolecithin-induced demyelination. *Neuropathol Appl Neurobiol, 25*(3), 226-235. doi:10.1046/j.1365-2990.1999.00172.x

Yin, F., Zhang, J. N., Wang, S. W., Zhou, C. H., Zhao, M. M., Fan, W. H., . . . Liu, S. (2015). MiR-125a-3p regulates glioma apoptosis and invasion by regulating Nrg1. *PLoS One, 10*(1), e0116759. doi:10.1371/journal.pone.0116759

Zhang, J., Cheng, Y., Cui, W., Li, M., Li, B., & Guo, L. (2014). MicroRNA-155 modulates Th1 and Th17 cell differentiation and is associated with multiple sclerosis and experimental autoimmune encephalomyelitis. *J Neuroimmunol, 266*(1-2), 56-63. doi:10.1016/j.jneuroim.2013.09.019

Zhao, L., Hu, P., Zhou, Y., Purohit, J., & Hwang, D. (2011). NOD1 activation induces proinflammatory gene expression and insulin resistance in 3T3-L1 adipocytes. *Am J Physiol Endocrinol Metab, 301*(4), E587-598. doi:10.1152/ajpendo.00709.2010

Zhao, X., He, X., Han, X., Yu, Y., Ye, F., Chen, Y., . . . Lu, Q. R. (2010). MicroRNA-mediated control of oligodendrocyte differentiation. *Neuron, 65*(5), 612-626. doi:10.1016/j.neuron.2010.02.018

Figure legends

Figure 1. MiR-125a-3p is upregulated under non-repairing demyelinating conditions. (A) Expression levels of miR-125a-3p in MS active lesions compared to normal-appearing white/gray matter and healthy control. CC = control cohort; MS = multiple sclerosis patients; WM = white matter; GM = gray matter; NAWM = normal-appearing white matter; WML = white matter lesion; NAGM = normal-appearing gray matter; GML = gray matter lesion. (B) Paired analysis comparing the expression levels of miR-125a-3p in NAWM and WML in each patient. Paired Student t test; * $p < 0.05$. (C) Schematic representation of the LPC experimental protocol: acute demyelination was induced in 3-4 month-old C57BL/6 mice by bilateral stereotaxic microinjection of 1% lysolecithin (LPC) solution into subcortical white matter. (D) Expression of miR-125a-3p in PDGFRα^+ OPCs isolated from the corpus callosum of LPC- and saline-injected mice was measured by qRT-PCR at 5 days-post lesion (dpl). Data are the mean ± SEM of 4 animals per group. (E) Schematic representation of the EAE experimental protocol: EAE was induced in 9-week-old C57BL/6 mice by subcutaneous immunization with the MOG 35-55 peptide. (F) Expression of miR-125a-3p in PDGFRα^+ OPCs isolated from the spinal cord of EAE and control mice was measured by qRT-PCR at 50 days-post immunization (dpi). Unpaired Student's t test; *$p < 0.05$.

Figure 2. MiR-125a-3p over-expression inhibits OPC maturation and remyelination after lysolecithin-induced demyelination. (A) Schematic representation of the experimental plan: at 9 dpl, mice were injected with LV particles designed to over-express miR-125a-3p (LV-miR-125a-GFP) or with control virus (LV-ctrl-GFP); (B) Gallyas myelin staining (brown) reveals the area of demyelination in the subcortical white matter at 5 dpl; (C-D) Immunofluorescence shows the distribution of GSTpi$^+$ mature oligodendrocytes and NG2$^+$ immature OPCs in the lesioned white matter at the same time-point; (E) Immunofluorescence shows the distribution of GFP$^+$ infected cells at 21 dpl; (F) Colocalization of NG2 (red) in GFP$^+$ (green)/Sox10$^+$ (cyan) cells infected by LV-miR-125a; (G) Colocalization of GSTpi (red) in GFP$^+$ (green)/Sox10$^+$ (cyan) cells infected by LV-ctrl; (H, I)

Quantification of NG2 or GSTpi co-expression in GFP$^+$ oligodendroglial (SOX10$^+$) cells at 21 dpl. Data are the mean ± SEM of 4 animals/group; Unpaired Student's t test; *p < 0.05; ***p < 0.001; (J) Quantification of myelin (Gallyas staining) in the lesioned area after LV-miR-125a-GFP or LV-ctrl-GFP infection (21 dpl). Abbreviations: CC, corpus callosum; V, lateral ventricle; SE, standard error; Scale bars: 50 µm in C, D; 500 µm in B, E; 20 µm in F, G.

Figure 3. MiR-125a-3p silencing accelerates *in vivo* and *ex vivo* remyelination after lysolecithin-induced demyelination. (A) Schematic representation of the experimental plan: at 5 dpl, mice were injected with LV particles designed to inhibit miR-125a-3p (LV-decoy-miR-125a) or with a control virus (LV-ctrl); (B, C) Representative micrographs of GSTpi$^+$ cell density in the lesioned area after LV-decoy-miR-125a or LV-ctrl infection at 21 dpl; (D,E) Quantification of GSTpi$^+$ and SOX10$^+$ cell density in the lesioned area after LV-decoy-miR-125a or LV-ctrl infection (21 dpl); (F, G) Representative micrographs of Gallyas myelin staining in the lesioned area after LV-decoy-miR-125a or LV-ctrl infection at 21 dpl; (H) Quantification of myelin in the lesioned area after LV-decoy-miR-125a or LV-ctrl infection (21 dpl); (I) Schematic representation of the ex-vivo demyelination protocol in cerebellar organotypic slices in which LV particles designed to inhibit miR-125a-3p were added to the medium; (J) Quantification of Olig2, Ng2, Olig1, Gpr17, Plp1 and Mbp mRNA levels at 12 days *in vitro* (div) was assessed by qRT-PCR. Data are the mean ± SEM of 4-5 animals; unpaired Student's t test; *p < 0.05; **p < 0.01. Scale bars: 50 µm in B, C.

Figure 4. Selection and validation of miR-125a-3p potential targets. (A) Heat map showing the expression of the top 50 up-regulated genes during OPC maturation (Dugas et al., 2006) after over-expression of miR-125a-3p (X125_1 and X125_2) compared to negative controls (NEG_1 and NEG_2). Down-regulated genes are in pink, whereas up-regulated genes are in green. (B) Venn diagram comparing computationally predicted target of miR-125a-3p by miRwalk (green), with genes down-regulated following miR-125a-3p over-expression in OPCs (blue), and genes whose expression is physiologically increased during OPC maturation (yellow; (Cahoy et al., 2008)). (C) Relative expression of Nod1, Gas7, Slc8a3 and Mbp after miR-125a-3p over-expression in OPCs. Data are the mean ± SEM of 5 independent experiments. Unpaired Student's t test; *** p < 0.001. (D, E) Histograms showing the expression pattern of Gas7 and Nod1 during *in vitro* OPC physiological maturation. One-way ANOVA with Tukey's multiple comparisons test, ** p < 0.01; *** p < 0.001.

Figure 5. MiR-125a-3p represses MBP expression by targeting Gas7 and Slc8a3 transcripts. Histograms showing the expression levels of Mbp (A) and the number of MBP$^+$ cells (B) after silencing

of Nod1, Gas7 or transfection of miR-125a-3p mimics in cultured OPCs compared to control (OPCs transfected with scramble RNA). One-way ANOVA with Tukey's multiple comparisons test. ** $p < 0.01$; *** $p < 0.001$ compared to control (CTL, scramble RNA transfection). (C-F) Representative micrographs showing MBP^+ cells (red) per field (20X magnification) after silencing of Nod1 or Gas7 and transfection of miR-125a-3p compared to CTL. Scale bar: 100µm. (G) Control plasmid, Gas7, Nod1 or Slc8a3 3'-UTR luciferase reporter vectors were transfected in COS7 cells with either miR-125a-3p mimics or scramble negative control (set to 100%). The dual luciferase assay was performed 48 hours after transfection. Gray and black bars indicate luciferase activity with the negative control (set to 100% in each condition) and miR-125a-3p, respectively. Data are presented as mean ± SEM from 5 experiments performed in triplicate and normalized to the effect of scramble RNA co-transfection. Two-way ANOVA with Tukey's multiple comparisons test, *** $p < 0.001$, **** $p < 0.0001$. (H) Schematic representation of the putative miRNA response element (MRE) for miR-125a-3p in the Slc8a3 3'-UTR. CDS = coding sequence; UTR = untranslated region. (I) Schematic representation of the Slc8a3 3'-UTR indicating the mutated MRE (red nucleotides). (J) Wild-type (light grey bars) and mutated (dark grey bars) Slc8a3 3'-UTR luciferase reporter vectors were transfected in COS7 cells with either miR-125a-3p mimics or scramble negative control. In each experimental group, the luciferase activity from the wild type 3'UTR was set to 100%. Data are presented as mean ± SEM from 5 experiments performed in duplicate. Unpaired Student's t test; *** $p < 0.001$.

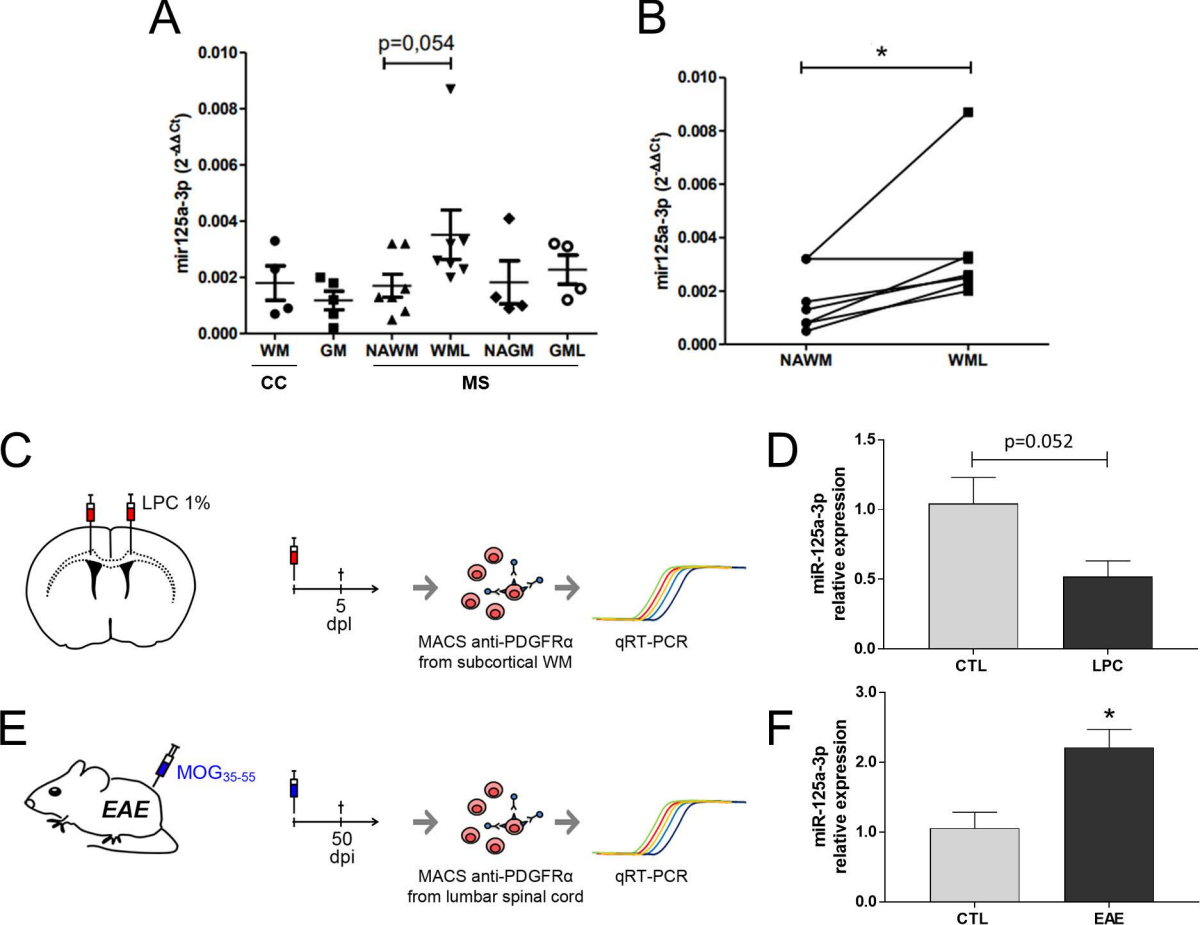
A
p=0,054
mir125a-3p (2^-ΔΔCt)
0.010
0.008
0.006
0.004
0.002
0.000
WM
GM
NAWM
WML
NAGM
GML
CC
MS
B
*
mir125a-3p (2^-ΔΔCt)
NAWM
WML
C
LPC 1%
5 dpl
MACS anti-PDGFRα from subcortical WM
qRT-PCR
D
p=0.052
miR-125a-3p relative expression
1.5
1.0
0.5
0.0
CTL
LPC
E
MOG35-55
EAE
50 dpi
MACS anti-PDGFRα from lumbar spinal cord
qRT-PCR
F
*
miR-125a-3p relative expression
3.0
2.0
1.0
0.0
CTL
EAE

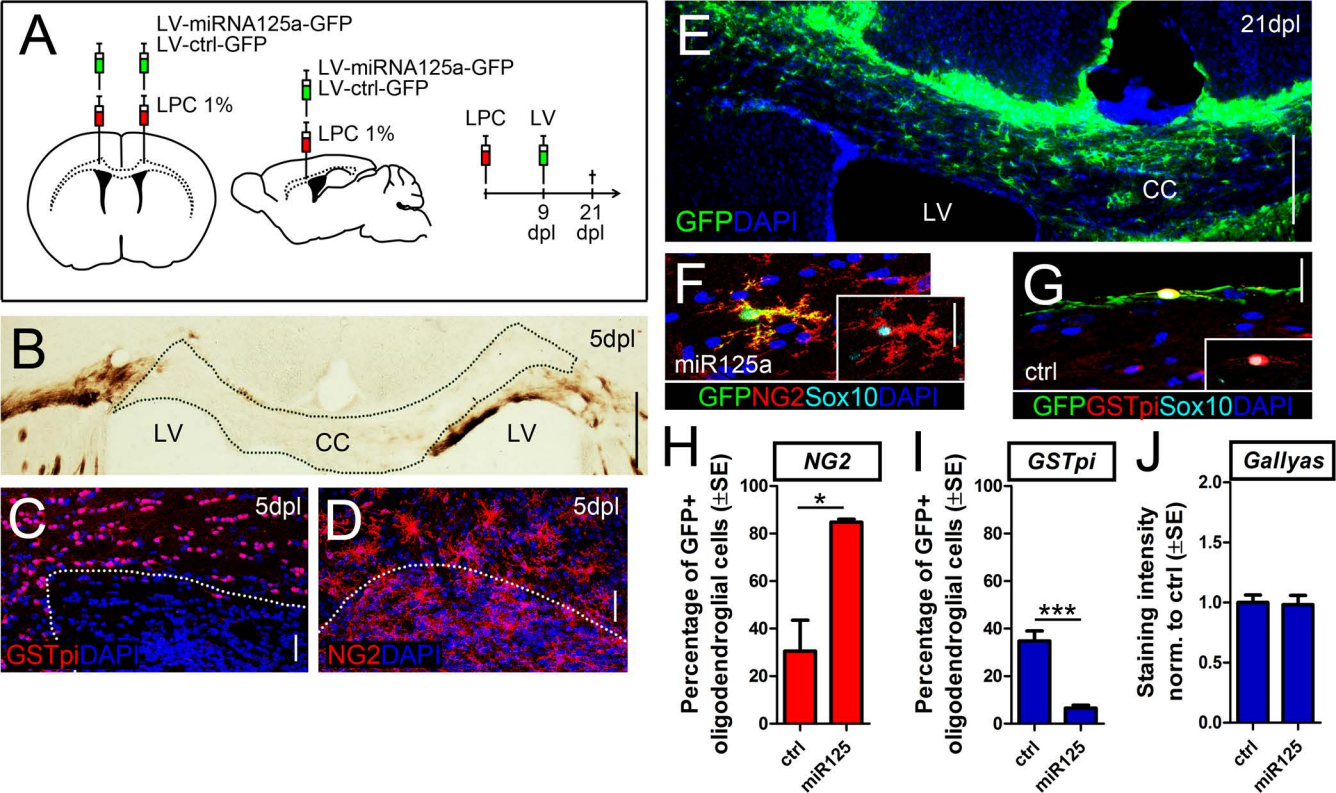
A
LV-miRNA125a-GFP
LV-ctrl-GFP
LPC 1%
LV-miRNA125a-GFP
LV-ctrl-GFP
LPC 1%
LPC
LV
9 dpl
21 dpl
B
5dpl
LV
CC
LV
C
5dpl
GSTpiDAPI
D
5dpl
NG2DAPI
E
21dpl
GFPDAPI
LV
CC
F
miR125a
GFPNG2Sox10DAPI
G
ctrl
GFPGSTpiSox10DAPI
H
NG2
Percentage of GFP+ oligodendroglial cells (±SE)
100
80
60
40
20
0
*
ctrl
miR125
I
GSTpi
Percentage of GFP+ oligodendroglial cells (±SE)
100
80
60
40
20
0
***
ctrl
miR125
J
Gallyas
Staining intensity norm. to ctrl (±SE)
2.0
1.5
1.0
0.5
0.0
ctrl
miR125

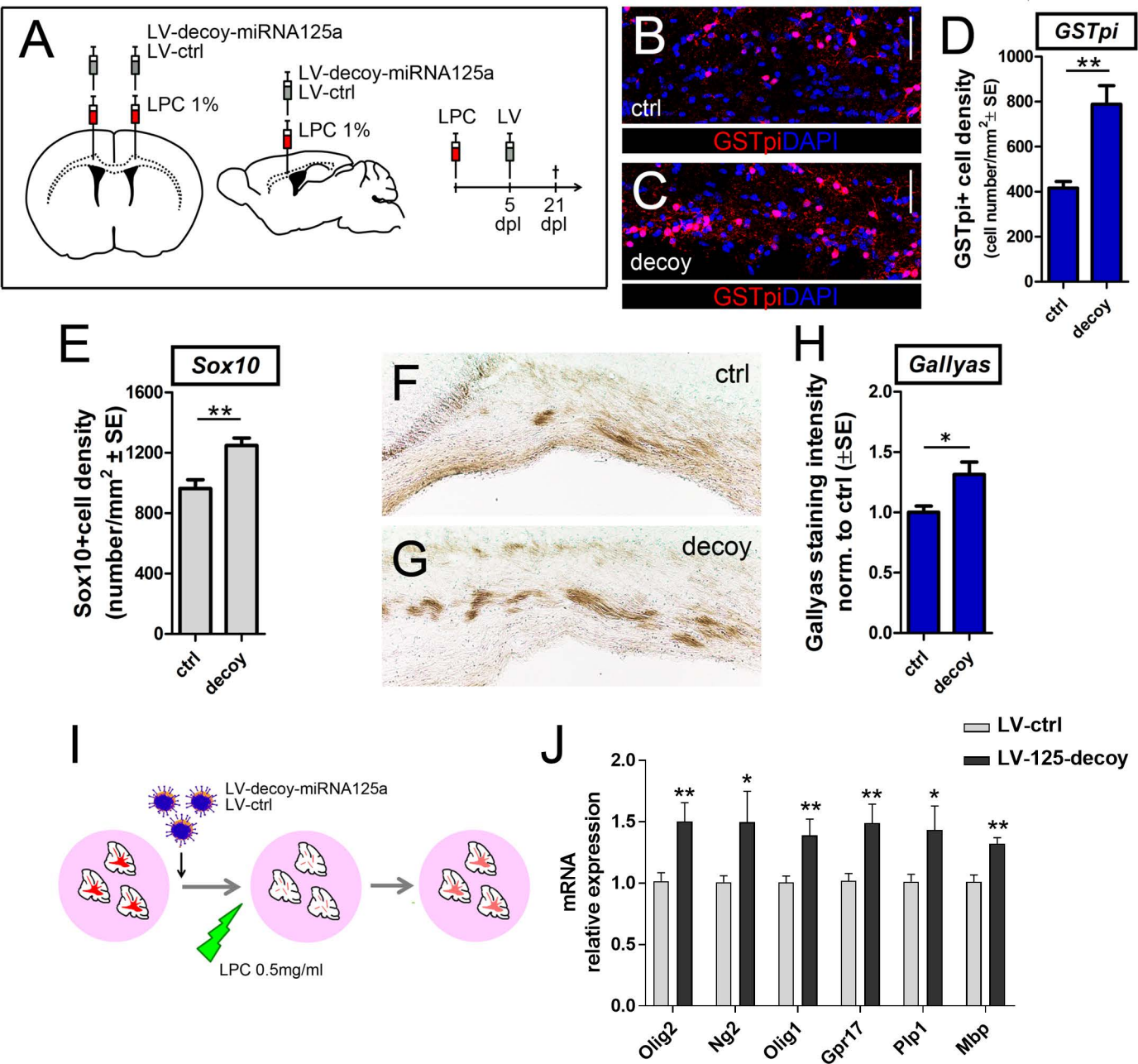
A
LV-decoy-miRNA125a
LV-ctrl
LPC 1%
LV-decoy-miRNA125a
LV-ctrl
LPC 1%
LPC
LV
5 dpl
21 dpl
B
ctrl
GSTpiDAPI
C
decoy
GSTpiDAPI
D
GSTpi
GSTpi+ cell density (cell number/mm2 ± SE)
1000
800
600
400
200
0
**
ctrl
decoy
E
Sox10
Sox10+cell density (number/mm2 ± SE)
1600
1200
800
400
0
**
ctrl
decoy
F
ctrl
G
decoy
H
Gallyas
Gallyas staining intensity norm. to ctrl (±SE)
2.0
1.5
1.0
0.5
0.0
*
ctrl
decoy
I
LV-decoy-miRNA125a
LV-ctrl
LPC 0.5mg/ml
J
LV-ctrl
LV-125-decoy
mRNA relative expression
2.0
1.5
1.0
0.5
0.0
**
*
**
**
*
**
Olig2
Ng2
Olig1
Gpr17
Plp1
Mbp

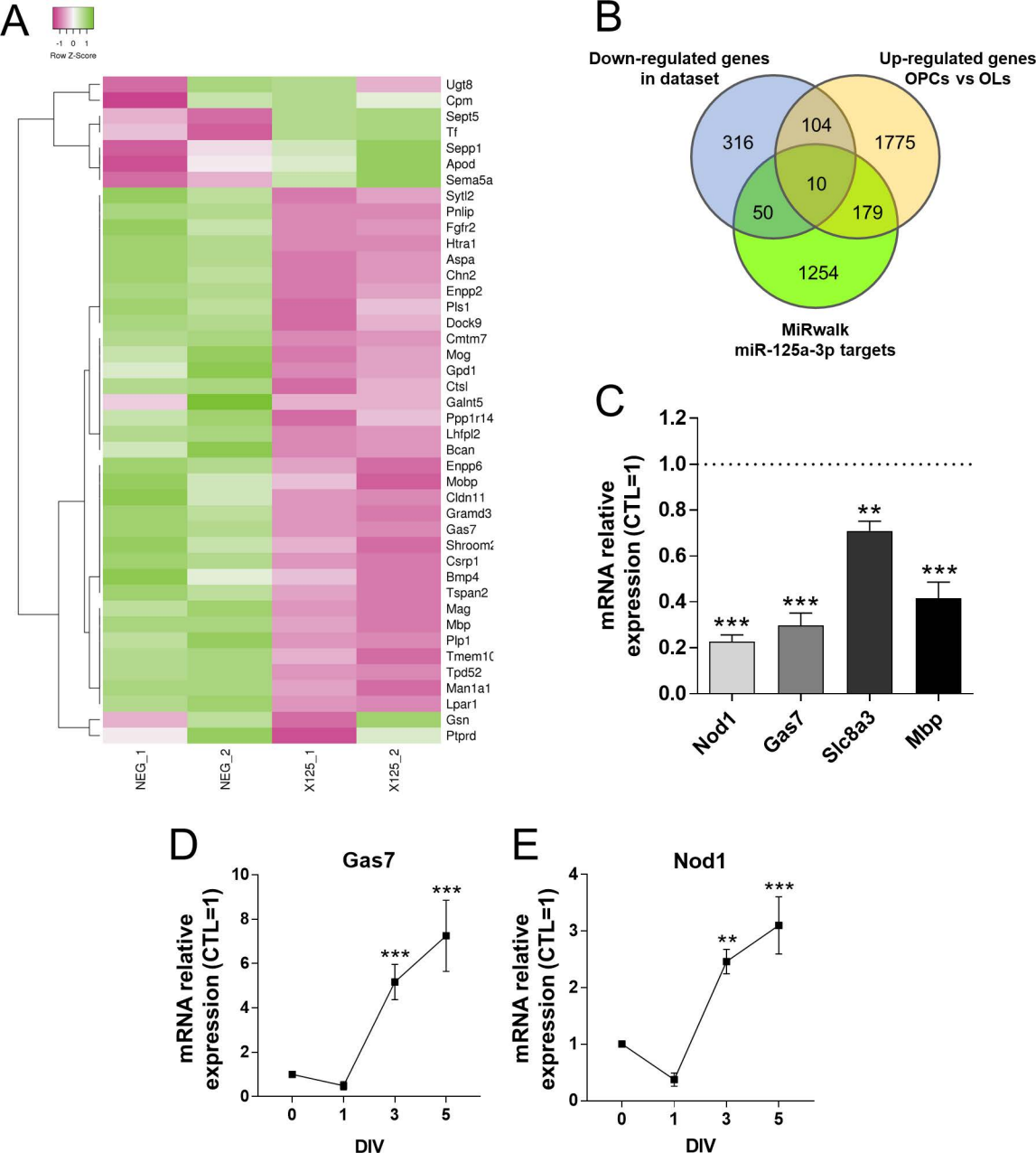
A
-1 0 1
Row Z-Score
Ugt8
Cpm
Sept5
Tf
Sepp1
Apod
Sema5a
Sytl2
Pnlip
Fgfr2
Htra1
Aspa
Chn2
Enpp2
Pls1
Dock9
Cmtm7
Mog
Gpd1
Ctsl
Galnt5
Ppp1r14
Lhfpl2
Bcan
Enpp6
Mobp
Cldn11
Gramd3
Gas7
Csrp1
Bmp4
Tspan2
Mag
Mbp
Plp1
Tpd52
Man1a1
Lpar1
Gsn
Ptprd
NEG_1
NEG_2
X125_1
X125_2
B
Down-regulated genes in dataset
Up-regulated genes OPCs vs OLs
MiRwalk miR-125a-3p targets
316
104
1775
10
50
179
1254
C
mRNA relative expression (CTL=1)
1.2
1.0
0.8
0.6
0.4
0.2
0.0
***
***
**
***
Nod1
Gas7
Slc8a3
Mbp
D
Gas7
mRNA relative expression (CTL=1)
10
8
6
4
2
0
***
***
0
1
3
5
DIV
E
Nod1
mRNA relative expression (CTL=1)
4
3
2
1
0
**
***
0
1
3
5
DIV

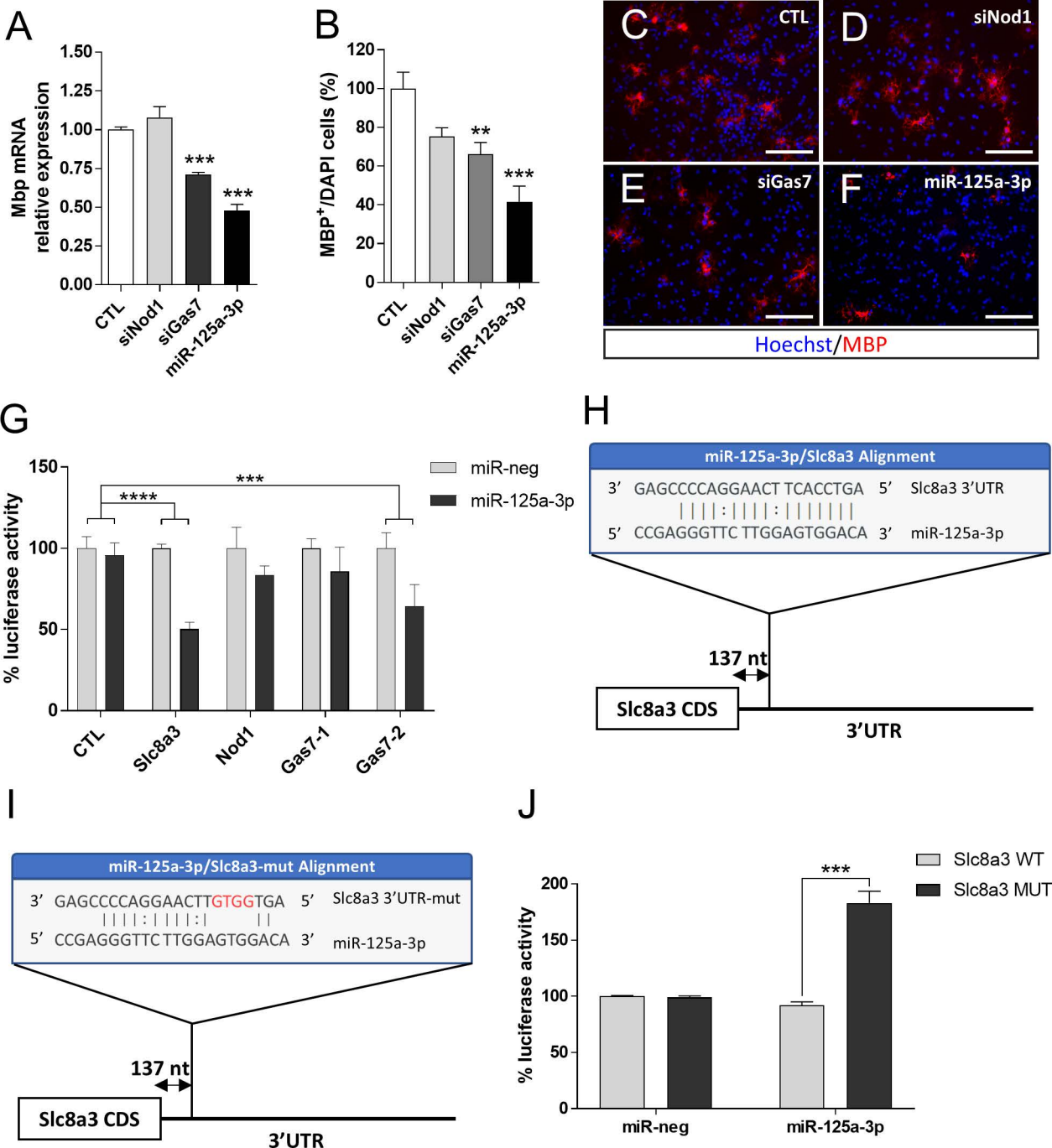
A
Mbp mRNA relative expression
1.50
1.25
1.00
0.75
0.50
0.25
0.00
***
***
CTL
siNod1
siGas7
miR-125a-3p
B
MBP+/DAPI cells (%)
120
100
80
60
40
20
0
**
***
CTL
siNod1
siGas7
miR-125a-3p
C
CTL
D
siNod1
E
siGas7
F
miR-125a-3p
Hoechst/MBP
G
% luciferase activity
150
100
50
0
miR-neg
miR-125a-3p
***
****
CTL
Slc8a3
Nod1
Gas7-1
Gas7-2
H
miR-125a-3p/Slc8a3 Alignment
3' GAGCCCCAGGAACT TCACCTGA 5' Slc8a3 3'UTR
5' CCGAGGGTTC TTGGAGTGGACA 3' miR-125a-3p
137 nt
Slc8a3 CDS
3'UTR
I
miR-125a-3p/Slc8a3-mut Alignment
3' GAGCCCCAGGAACTTGTGGTGA 5' Slc8a3 3'UTR-mut
5' CCGAGGGTTC TTGGAGTGGACA 3' miR-125a-3p
137 nt
Slc8a3 CDS
3'UTR
J
% luciferase activity
200
150
100
50
0
Slc8a3 WT
Slc8a3 MUT
***
miR-neg
miR-125a-3p

Supplementary material

Case	Gender	Diagnosis	Disease length (years)	Age of death	Cause of death	Post-mortem delay (hours)
C08	F	CC	-	93	Broncho-pneumonia, cerebro-vascular accident	9
C14	M	CC	-	64	Cardiac failure	18
C15	M	CC	-	82	-	21
C22	F	CC	-	69	Lung cancer	33
C25	M	CC	-	35	Carcinoma of tongue	22
MS122	M	SPMS	-	44	Broncho-pneumonia	16
MS163	F	SPMS	6	45	Multi-organ failure septicaemia due to urinary tract infection, MS	28
MS166	F	SPMS	36	62	Broncho-pneumonia, MS	7
MS200	F	SPMS	19	44	Urinary tract infection, sepsis, MS	20
MS245	M	SPMS	26	64	Broncho-pneumonia, MS	25
MS383	M	PPMS	8	42	Aspiration pneumonia	17
MS473	F	PPMS	13	39	Broncho-pneumonia, MS	9

Table S1. Demographic and clinical data of examined MS patients and control cases, obtained by the UK MS Tissue Bank. Case indicated with * have been excluded from this study for technical reasons. [F=female; M=male; CC=control case; MS=multiple sclerosis; SPMS=secondary progressive multiple sclerosis; PPMS=primary progressive multiple sclerosis].

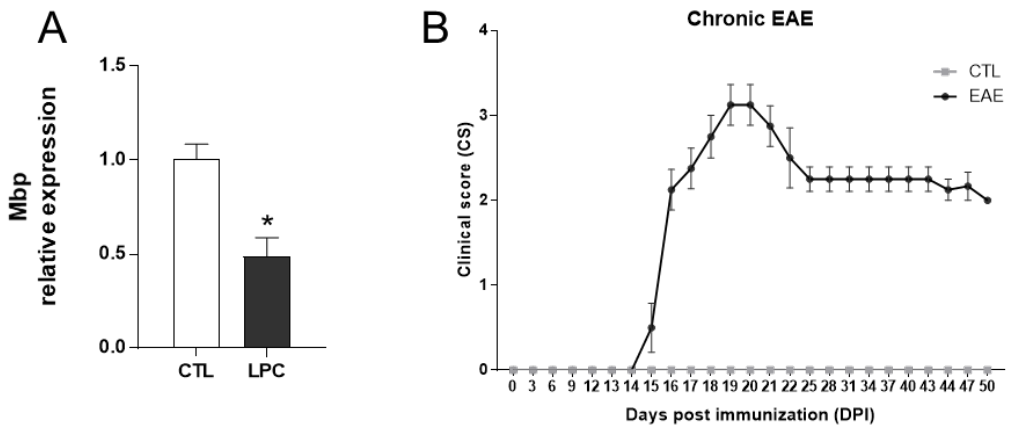

Figure S1. (A) Expression of MBP in the corpus callosum at 5 days post-lesion (dpl) was measured by qRT-PCR. Data are the mean ± SEM of 4-5 animals. Unpaired Student's t test; *$p < 0.05$. (B) Clinical scores of mice during chronic EAE. Error bars represent mean of CS ± SEM. Data are the mean ± SEM of 4 animals.

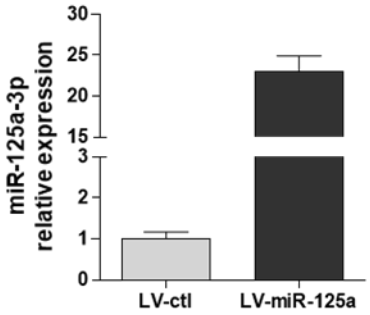

Figure S2. Expression of miR-125a-3p in mixed glial cells transduced with LV-miR-125a-GFP compared to LV-ctrl-GFP.

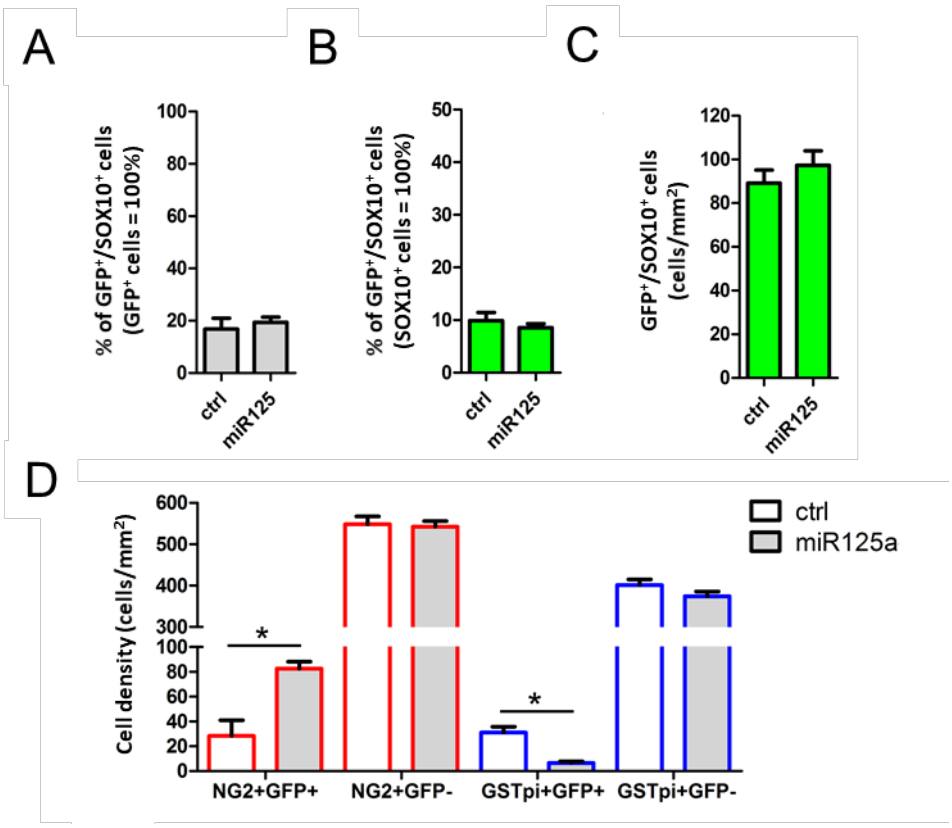

Figure S3. Percentage of SOX10/GFP double-positive cells over the GFP$^+$ cells (A) and over the SOX10$^+$ oligodendrocytes (B) in the experimental groups. (C) Quantification of GFP$^+$/SOX10$^+$ cells in the experimental groups. (D) Analysis of the maturation state of GFP$^+$ and GFP$^-$ oligodendrocytes in the experimental groups.

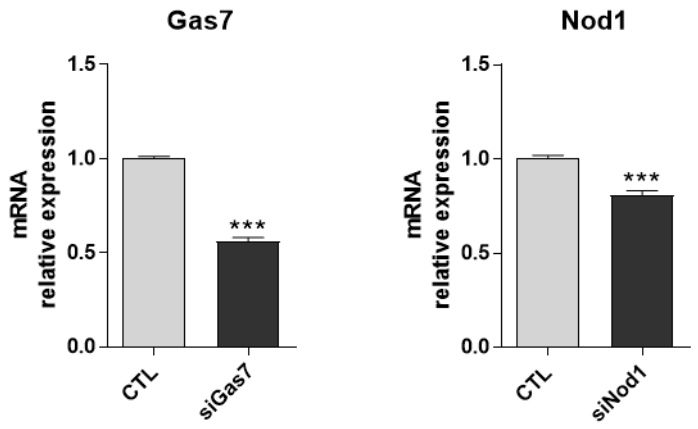

Figure S4. Expression of Gas7 and Nod1 mRNA in OPCs at 48 hours post-transfection of small interference RNA specific for Gas7 and Nod1 transcript, respectively.

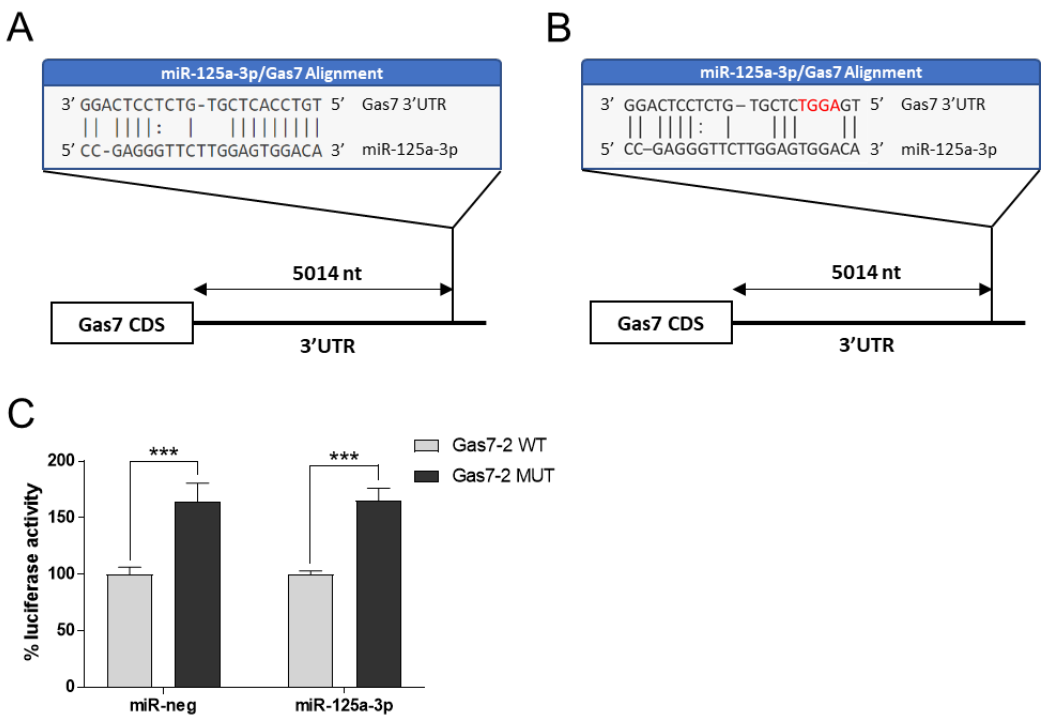

Figure S5. (A) Schematic representation of the putative miRNA response element (MRE) for miR-125a-3p in the Gas7 3'-UTR. CDS = coding sequence; UTR = untranslated region. (B) Schematic representation of the Gas7 3'-UTR indicating the mutated MRE (red nucleotides). (C) Wild-type Gas7 3'-UTR (light grey) and Gas7 3'UTR-mut (dark grey) luciferase reporter vectors were transfected in COS7 cells with either miR-125a-3p mimics or scramble negative control. In each experimental group, the luciferase activity from the wild type 3'UTR was set to 100%. Unpaired Student's t test; *** $p < 0.001$.

Gene name	Abundance in CTL	Abundance in miR-125a-3p	Fold change
Nod1	1.78	-0.34	-4.36
Epha4	-5.20	-6.98	-3.44
Mylk	-3.14	-4.72	-2.98
Slc8a3	-4.86	-6.38	-2.86
Gas7	1.18	-0.19	-2.59
Ccnjl	3.88	3.03	-1.81
Myo1d	1.99	1.19	-1.74
Mapre1	6.64	5.86	-1.71
Hist3h2ba	5.44	4.75	-1.62
Ttyh2	3.63	2.94	-1.60

Table S2. Table showing abundance and fold change of the 10 overlapping genes coming from the *in-silico* comparative

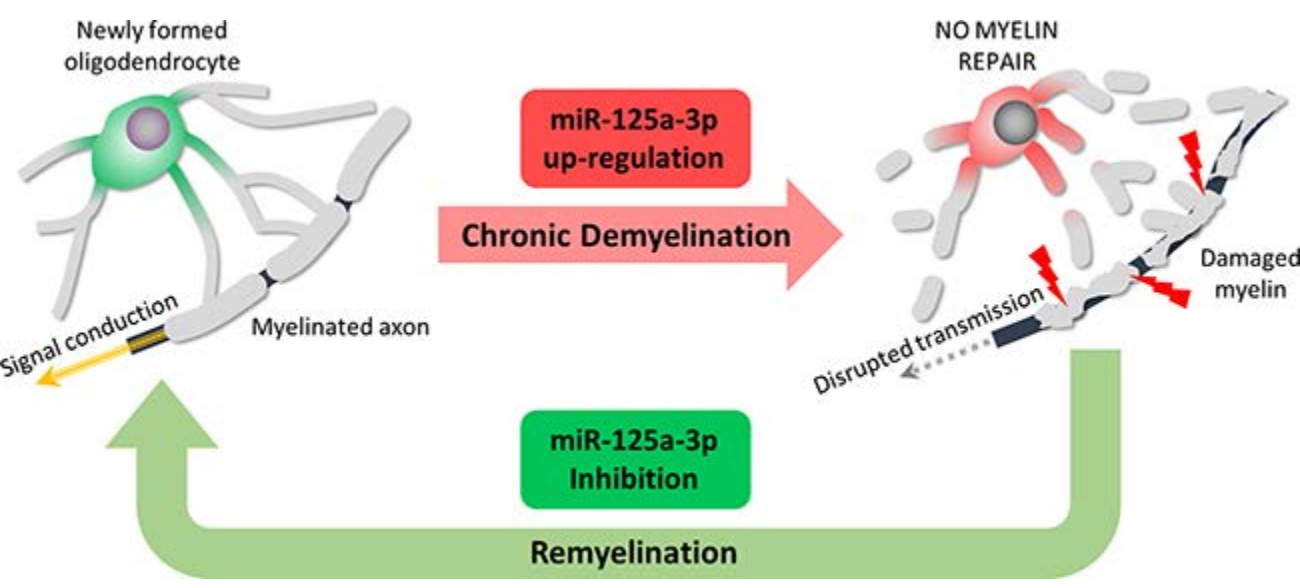
Newly formed
oligodendrocyte
Signal conduction
Myelinated axon
miR-125a-3p
up-regulation
Chronic Demyelination
NO MYELIN
REPAIR
Damaged
myelin
Disrupted transmission
miR-125a-3p
Inhibition
Remyelination